Fall 2007

Transient performance of closed loop thermosyphons incorporating thermal storage

Kyle S. Benne

Department:

TRANSIENT PERFORMANCE OF CLOSED LOOP THERMOSYPHONS INCORPORATING THERMAL STORAGE

by

KYLE S. BENNE

A THESIS

Presented to the Faculty of the Graduate School of the

UNIVERSITY OF MISSOURI–ROLLA

In Partial Fulfillment of the Requirements for the Degree

MASTER OF SCIENCE IN MECHANICAL ENGINEERING

2007

Approved by

Kelly O. Homan, Advisor

David W. Riggins

Bassem F. Armaly

PUBLICATION THESIS OPTION

This thesis has been prepared in the form of two papers for publication. The first paper is contained within pages 2-37. The second paper is within pages 38-76. Both of these are to be submitted for publication in *Numerical Heat Transfer* and they are formatted in the appropriate style. A brief introduction to the content of these publications has been presented on page 1. Details that are omitted from the publications are included in the appendix starting on page 77.

ABSTRACT

This thesis considers a unique application of a thermosyphon to a conventional thermal storage device. In such an application, the dynamics of the thermosyphon are coupled with the condition of the storage volume. This thesis specifically focuses on the transient energy addition or charge process, where heat accumulated within the storage volume continuously decreases the driving buoyant force and volumetric flow rate. A numerical investigation is first carried out for a thermosyphon storage device with constant heat addition and it is determined that the decaying flow rate causes a less than uniform charge profile. The results indicate that the profile can be improved by targeting the frictional losses to the transitional regime and by decreasing the relative height of the heating portion of the thermosyphon loop. A second numerical investigation is carried out for a thermosyphon storage device with constant temperature heat addition. For this configuration, the storage temperature is, of course, limited by the temperature of the heat source; however, the decaying flow rate causes reduced power delivery to the storage volume. The results of the second investigation indicate that power delivery can be sustained by targeting the frictional loss to the transitional flow regime.

ACKNOWLEDGMENTS

I greatly appreciate the people who have contributed to my research. My sincerest gratitude goes to my advisor Dr. Kelly Homan. His mentorship has been essential and it will undoubtedly have lasting influence on my life and career. I would also like to express my appreciation for my graduate committee members Dr. Bassem Armaly and Dr. David Riggins.

I am especially grateful to my parents for guiding me and teaching me the value of hard work. To my brother for setting a good example. Finally, to my best friend and the love of my life, Ashley, for having infinite confidence in me and offering her endless support.

TABLE OF CONTENTS

LIST OF ILLUSTRATIONS

INTRODUCTION

Natural convection flow loops known as thermosyphons circulate fluid by utilizing the buoyant force generated by a temperature gradient. Because they eliminate the need for a mechanical pump, thermosyphons are particularly well suited for applications where low cost, energy efficiency, and reliability are important. The applications of thermosyphons are diverse and subsequently there is a broad body of relevant literature, yet the majority of these publications focus on the steady and small time scale behavior of the thermosyphon.

This thesis is motivated by the novel idea of integrating a thermosyphon within a conventional thermal storage device. Experiments have shown that utilization of the thermosyphon improves thermal performance by eliminating large scale thermal mixing. The focus of this thesis is on the heat addition or charge process of the thermosyphon storage device. During charging, the thermosyphon dynamics are inherently transient because they are coupled with the changing state of the storage volume. The thermosyphon storage device is modeled by numerically solving the relevant momentum and energy balance laws, which are coupled and unsteady. The numerical method is programmed using FORTRAN and included in the appendix.

There are two distinct investigations presented in this thesis. The first investigation pertains to a system with constant heat addition, such as an electric resistance heating element. The second investigation pertains to a system with constant temperature heat addition. The constant temperature condition simulates an energy storage device with a condensing heat exchanger as the heat source. The fundamental objective in both of these studies is to identify the relevant design parameters and determine their influence on the system performance. Particular emphasis is given to understanding the role of the frictional losses. In both studies, the dominant loss mechanism is used to tailor optimal system performance.

1. Dynamics of a Closed Loop Thermosyphon Incorporating Thermal Storage*

K. S. Benne and K. O. Homan†
Department of Mechanical & Aerospace Engineering
University of Missouri-Rolla, Rolla, Missouri 65409–0050
Tel: 573–341–6622, Fax: 573–341–4115
Email: khoman@umr.edu

Abbreviated Title: Storage Thermosyphon Dynamics.

*Submitted to *Numerical Heat Transfer, Part A Applications*, (Version 38).
†Author to whom correspondence should be addressed

Abstract

The coupling between a natural convection thermosyphon loop and a thermal storage device is analyzed numerically for a charging process in which energy is added to the system at a fixed rate. Since energy accumulates in the storage component, the driving buoyant force is continually altered and the behavior is inherently transient. The undesirable consequence is a less than uniform charge of the storage volume. Relevant dimensionless parameters are identified which enable improvement in the shape of the charge profile. The results indicate that a more uniform charge profile is obtained by targeting the frictional losses to the transitional regime and by decreasing the relative vertical height where heat input occurs.

1. INTRODUCTION

Natural convection flow loops known as thermosyphons eliminate the need for a conventional pump by using the buoyancy resulting from a temperature gradient to circulate fluid. Thermosyphons have been applied to a range of applications and are often found in situations where energy efficiency is a concern, or where low cost and low maintenance is desired [1]. Because of their wide range of applications, there is a large literature pertaining to them. Thermosyphon configurations are traditionally classified into closed loop and open loop geometries [2].

The open loop thermosyphon consists of one or more heating or cooling ducts, which draw fluid from one thermal reservoir and deliver to a second reservoir. In some configurations these volumes are combined and the fluid is drawn from the same vessel that it is returned to. In both situations, the sizes of the reservoirs are considered large enough to be unaffected by the heat addition or removal in the connecting duct. Because of this assumption, there exists a steady state solution to the system dynamics. Beginning from

such a solution, the initial transient and stability behavior of the open loop thermosyphon has been well studied, particularly in regard to geothermal applications [3, 4, 5].

The closed loop geometry continuously circulates fluid through a closed path with periodic heating or cooling sections. The majority of the literature pertaining to the closed loop thermosyphon implements the heating and cooling sections in a way which ensures that the net heat addition is balanced by the heat removal. This is accomplished by specifying balanced heat flux around the flow loop, or by incorporating at least one convective boundary within the system. The existence of a balanced heating load also makes it possible for a steady state solution to exist. Similar to that of the open loop thermosyphon, the initial transient and stability behavior have been investigated for this type of thermosyphon. Under certain conditions, theory and experiment show that some closed loop thermosyphons are unstable, resulting in repeated oscillations of the flow direction. A toroidal loop that is symmetrically heated from below and cooled from above has been found to be unstable at some heating rates [6, 7], although the stability was found to improve when the toroid was rotated such that the heating was not symmetric [8]. Similar conclusions have been reached using a Fourier expansion to reduce the governing conservation equations to a system of ordinary differential equations [9]. A Fourier expansion has been more recently used to design a control system that improves the stability of a toroidal thermosyphon [10], and a symmetric rectangular thermosyphon [11].

The focus of the present investigation is a thermosyphon with unbalanced heat addition in communication with a finite thermal reservoir which accounts for the majority of the system's volume. These features distinguish this investigation from those cited. The present configuration is distinct from the traditional open loop thermosyphon, because the thermal reservoir is finite; therefore, the condition of the reservoir is coupled with the dynamics of the thermosyphon. It is also distinct from the closed loop studies that have been mentioned, because there is net heat addition causing the energy inventory of the thermal reservoir to steadily increase. Because of these two characteristics, the steady state solution

that has been used as the basis of the preceding investigations is not applicable to the present configuration. The system is therefore inherently time dependent, and as a result, this study focuses on the unsteady dynamics of the energy addition process.

A common application of the general type of thermosyphon system being considered is in solar domestic hot water (SDHW) heating. This application contains the two features that are distinct to the thermosyphon system of present interest. The SDHW system incorporates a finite thermal storage tank, and during daytime heating there is an unbalanced energy addition as a result of the heat added by the solar collector. One configuration for this type of domestic hot water system is known as an indirect system because the storage volume is isolated from the thermosyphon loop by a heat exchanger. Numerous studies pertaining to variations of this type of device are reported in the literature [12, 13, 14, 15, 16]. Alternatively, a direct configuration has thermal storage integrated within the thermosyphon flow path. Studies pertaining to this type of system have also been carried out [17, 18].

Another application for the type of thermosyphon system being considered is a novel configuration of an electric resistance water heater (ERWH). This device consists of a thermal reservoir with a smaller duct intended to draw fluid from the lower portion of the storage vessel and deliver heated fluid to the upper portion. The duct, or riser section, is either internal or external to the main storage volume and contains a heating mechanism in its lower portion. This configuration avoids large-scale thermal mixing and maintains stratification within the storage volume by isolating the rising plume of heated fluid from the main storage volume. Previous work [19] has shown that in a system composed of a storage volume and an electric resistance heating element, elimination of the large-scale thermal mixing in the storage vessel leads to significant improvements in performance, both for charging processes and discharging processes. In addition, recent experimental work [20] demonstrated that conventional ERWH systems operate with a high degree of internal thermal mixing. A thermosyphon-based configuration avoids much of this internal thermal mixing and enables significant improvements in performance [21].

The present investigation focuses specifically on the tailoring of the system dynamics so as to approach a process in which the storage volume is heated to a specific uniform temperature. To accomplish this goal, the thermosyphon must deliver steady flow through the system so that a consistent temperature rise is achieved across the heating portion of the loop, given a constant heat input rate. This is an elusive goal, because the changing temperature profile of the thermal storage component affects the buoyant force circulating the fluid [22]. In this study, the controlling design parameters are identified and their effects on the temperature profile of the storage are determined. Our results show that most of the primary system parameters, when grouped into a single dimensionless term, have almost no impact on the shape of the riser outlet temperature profile. However, the shape of the riser outlet temperature profile can be favorably modified by the vertical length of the heating section and the flow regime in the dominant flow restriction.

2. PROBLEM FORMULATION

2.1 Problem Description

A thermosyphon composed of three distinct sections is used as the basis of the analysis in this study. The components are a storage section, a heating section composed of an electric resistance device, and a flow restriction. A conceptual schematic identifying these pieces is given by Figure 1. The heating and resistance sections form the riser of the thermosyphon and the storage volume is the sole component of the downcomer. Gravity is everywhere pointing downward. Fluid is drawn into the riser from the bottom of the storage vessel, heated, and returned to the top of the storage. The entire system is adiabatic except for the heat input section. This configuration simulates a thermal charge process where the energy inventory of the storage volume is continuously increasing. The flow restriction section is the single throttling mechanism of the loop. The other components are presumed to have comparatively larger cross sectional areas, therefore the magnitude of the flow resistance is much smaller and is neglected. While neglecting the frictional loss in

all but one part of the loop is an approximation, it is consistent with the intent of having a dominant flow restriction and allows the effects of a specific flow regime to be studied. The geometry of the restriction section is used to control the flow rate of the thermosyphon loop, and as a result affects the temperature rise across the heating section. We will later show that specific flow regimes will deliver improved transient performance. Once an optimal flow regime is identified, a physical design can be implemented that is dominated by this flow regime.

A quasi one-dimensional model, illustrated by Figure 2, is used to simulate the thermosyphon system just described. In this model there is a single spatial coordinate representing the position around the loop. The cross sectional area of the flow path is a function of this coordinate. The spatial coordinate, s, begins at the entrance to the heating section and extends to the outlet of the storage volume where the loop is then closed. The overall height of the system, $\hat{H}$, is equivalent to the height of the storage tank. The heat input and restriction sections are vertically confined within the storage volume, however they may be physically positioned inside or outside of this component. In the present model only the vertical components are recognized, and as a result the horizontal position of the components is irrelevant. The lengths of the heating and the restriction sections are $\hat{l}_h$ and $\hat{l}_r$ respectively. The length of the riser is equal to the overall system height, but as indicated by Figure 2 this is not necessarily the sum of $\hat{l}_h$ and $\hat{l}_r$. The heating section begins at the base of the riser and the restriction section ends at the outlet of the riser. The length separating these two components floats to allow the riser to extend the full height of the system. The total length of the flow loop is $2\hat{H}$.

2.2 Equation Development

The governing momentum balance is developed beginning from a differential element of the system and then integrating around the loop. The pressure and flux terms are continuous functions of the spatial coordinate and they are eliminated by integrating around

the closed path. In dimensional form, the momentum equation simplifies to

$$\left(\int_0^{2\hat{H}} \frac{d\hat{s}}{\hat{A}}\right) \frac{d\hat{\dot{V}}}{d\hat{t}} = -\int_0^{2\hat{H}} \frac{4\hat{\tau}_w}{\rho_o \hat{D}_h} d\hat{s} + g\beta \int_0^{2\hat{H}} \left(\hat{T} - \hat{T}_o\right) G(\hat{s}) d\hat{s}, \tag{1}$$

where $G(\hat{s})$ indicates the orientation of a particular section of the flow loop with respect to gravity. It is taken to be positive one in the riser portion of the loop ($0 \leq \hat{s} < \hat{H}$) and negative one in the downcomer ($\hat{H} \leq \hat{s} < 2\hat{H}$). The dimensional volumetric flow rate is denoted by $\hat{\dot{V}}$, the dimensional cross-sectional area by $\hat{A}$, and the dimensional temperature by $\hat{T}$. Within the frictional loss term, D_h represents the conventional hydraulic diameter. The initial temperature is denoted by $\hat{T}_o$. The cross-sectional area varies significantly with position, $\hat{A} = \hat{A}(\hat{s})$, while the volumetric flow rate varies only in time, $\hat{\dot{V}} = \hat{\dot{V}}(\hat{t})$, as dictated by conservation of mass. The temperature varies with space and time, $\hat{T} = \hat{T}(\hat{t}, \hat{s})$. The wall shear stress in the throttling section is defined as

$$\hat{\tau}_w = \frac{1}{2} \rho_o \hat{v}^2 \lambda, \tag{2}$$

where $\hat{v}$ is the local velocity and λ is the Fanning friction factor, a function of Reynolds number, $\lambda = \lambda(Re)$. The functional dependence of the friction coefficient on the Reynolds number is based on the fluid flow regime and is represented by the general form,

$$\lambda = \frac{a}{Re^b} + c. \tag{3}$$

The temperature profile within the flow loop is described by a one dimensional energy balance that includes the effects of diffusion due to conduction in the axial direction.

Energy is added to the system only within the heating portion of the thermosyphon loop. The resulting differential energy equation is

$$\rho c_p \frac{\partial}{\partial \hat{t}}(\hat{A}\hat{T}) + \rho c_p \frac{\partial}{\partial \hat{s}}(\hat{A}\hat{v}\hat{T}) = \hat{\dot{W}}_e'(s) + \frac{\partial}{\partial \hat{s}}\left(k\hat{A}\frac{\partial \hat{T}}{\partial \hat{s}}\right). \tag{4}$$

2.3 Non-dimensionalization

The dimensional forms of the governing equations can be specialized for the intended application by choosing appropriate dimensional scales. The intent of the present application is to heat a liquid, such as water, from a minimum starting temperature to a specified set point temperature. Symbolically this temperature difference is represented as $\Delta\hat{T}_{sp} = \hat{T}_{sp} - \hat{T}_o$. The dimensionless temperature, T, is defined according to $\hat{T} = \Delta\hat{T}_{sp}T + \hat{T}_o$, therefore the setpoint temperature is achieved at $T = 1$. The time scale is chosen as the time required to uniformly charge the storage volume to the setpoint temperature using all of the available heating power. Symbolically the dimensionless time is defined as,

$$t = \frac{\hat{t}}{\rho c_p \hat{V}_s \Delta\hat{T}_{sp}/\hat{\dot{W}}_e}, \tag{5}$$

where $\hat{V}_s$ is the dimensional storage volume and $\hat{\dot{W}}_e$ is the electric energy transfer rate to the resistance element. The nominal volumetric flow rate would be a circulation of one storage volume through the heating section of the loop during the time of one charge cycle. This volumetric flow rate is referred to as the characteristic flow rate and is defined by

$$\hat{\dot{V}}_o = \frac{\hat{V}_s}{\rho c_p \hat{V}_s \Delta\hat{T}_{sp}/\hat{\dot{W}}_e}. \tag{6}$$

The characteristic flow rate is a natural scaling choice for the dimensionless volumetric flow rate, $\dot{V} = \hat{\dot{V}}/\hat{\dot{V}}_o$. The length scale is selected as the overall height of the system, $\hat{H}$, which

reflects both the height of the storage vessel and the height of the riser. The cross sectional area is scaled by the diameter of the storage vessel.

Applying the preceding dimensional scales to the governing momentum equation and identifying significant parameter groups results in a momentum balance in the form

$$\begin{aligned} \frac{R_s^2 Re_o^2}{Gr}\left[\int_0^2 \left(\frac{D_r}{D}\right)^2 ds\right]\frac{d\dot{V}}{dt} &= \\ -2\frac{R_s^3 Re_o^2}{Gr}\left[\int_0^2 \frac{D_r^2}{D^5}F(s)ds\right]\lambda\dot{V}^2 &+ \int_0^2 G(s)Tds, \end{aligned} \tag{7}$$

where $s \equiv \hat{s}/\hat{H}$, $D(s) \equiv \hat{D}(s)/\hat{D}_s$, and $\hat{D}_s$ is the diameter of the storage vessel. The Reynolds number, Re_o, is a nominal value based on the characteristic flow rate passing through the restriction section. Symbolically this is

$$Re_o = \frac{4\hat{\dot{V}}_o}{\pi \hat{D}_r \nu}, \tag{8}$$

where $\hat{D}_r$ is the dimensional diameter of the flow restriction section. The true Reynolds number at any instant in time during the simulation is given by $Re = \dot{V} Re_o$. The Grashoff number, Gr, is defined as

$$Gr = \frac{g\beta \Delta \hat{T}_{sp} \hat{H}^3}{\nu^2}. \tag{9}$$

The remaining symbol, R_s denotes the aspect ratio of the storage vessel and it is defined as $R_s \equiv \hat{H}/\hat{D}_s$. The term $F(s)$ is used as a switch to turn the frictional flow resistance on and off along the flow path. Presently, only the losses in the designated restriction section are recognized, therefore this term takes on the value of one within the flow restriction and zero elsewhere. Using this assumption the dimensionless momentum equation reduces to

$$\begin{aligned} \frac{R_s^2 Re_o^2}{Gr}\left[\int_0^2 \left(\frac{D_r}{D}\right)^2 ds\right]\frac{d\dot{V}}{dt} &= \\ -\left(2\frac{R_s^3 Re_o^2 l_r}{Gr\, D_r^3}\right)\lambda\dot{V}^2 &+ \int_0^2 G(s)Tds, \end{aligned} \tag{10}$$

where $l_r \equiv \hat{l}_r / \hat{H}$ is the dimensionless length of the flow resistance section. In order to make the previous equation more compact, a parameter Γ is defined according to,

$$\Gamma = 2 \frac{R_s^3 Re_o^2 l_r}{Gr D_r^3}. \tag{11}$$

Physically this term represents a ratio between frictional flow resistance and driving buoyant force. Upon substitution, the momentum equation becomes

$$\frac{R_s^2 Re_o^2}{Gr} \left[\int_0^2 \left(\frac{D_r}{D} \right)^2 ds \right] \frac{d\dot{V}}{dt} = -\Gamma \lambda \dot{V}^2 + \int_0^2 G(s) T ds. \tag{12}$$

Applying the same dimensional scales and again grouping significant parameters, the dimensionless form of the energy equation is

$$\frac{\partial T}{\partial t} + \frac{\dot{V}}{D^2} \frac{\partial T}{\partial s} = \frac{J(s)}{l_h D^2} + \frac{1}{Pe D^2} \frac{\partial}{\partial s} \left(D^2 \frac{\partial T}{\partial s} \right), \tag{13}$$

where $l_h \equiv \hat{l}_h / \hat{H}$ is the dimensionless length of the heating section. In a manner similar to $F(s)$, a binary heat input function, $J(s)$, is used to specify the location of heat input in the flow loop. This term takes on the value of one within the heating section and zero elsewhere. The Peclet number, Pe, is defined as

$$Pe = \frac{4 \hat{\dot{V}}_o \hat{H}}{\pi \hat{D}_s^2 \alpha}. \tag{14}$$

Defined in this way, the Peclet number reflects the ratio of diffusion time relative to advection time through the storage vessel at the nominal flow rate.

2.4 Solution Method

The governing conservation equations are a coupled set composed of an ordinary differential equation and a partial differential equation. An analytical solution to this system of equations is not readily available. Previous work on similar problems has either reduced

the equations to a system of ordinary differential equations, or applied a numerical approach. The present study adopts a numerical technique.

The energy equation is solved with an implicit method using a central difference to approximate the diffusion term. The advection term of the energy equation is treated using a flux based approach, known as the monotonic piecewise linear (MPL) method [23]. This method provides second order accuracy for the advection term while avoiding the dispersion introduced by a central difference. The momentum equation is solved using the second order Adams Bashforth method with the buoyancy term lagged in time. In terms of numerical stability, the implicit method used to solve the energy equation avoids the timestep limitation otherwise imposed by the diffusion term, however the CFL condition still applies to the MPL and Adams Bashforth methods. This criteria significantly limits the size of the timestep, because of the small diameter and high velocity in the restriction section. In spite of this fact, the numerical computation is relatively inexpensive and a more advanced method is not required.

3. RESULTS AND DISCUSSION

3.1 Parameter Choices and Initial Design

The principle mechanisms governing the flow in the thermosyphon loop are a balance between the driving buoyant force and the frictional flow resistance. The parameters of the system must be chosen carefully so that the balance between these two forces will obtain the appropriate volumetric flow rate. In the present application this is particularly important, because with constant energy addition, it is the flow rate that prescribes the temperature rise across the heating section. As previously mentioned, the challenge posed by a thermosyphon loop that accumulates energy in the attached reservoir is that the driving buoyant force is continuously changing as the temperature increases in the system. In the present configuration, the primary energy storage is in the downcomer of the loop, therefore the consequence of heat addition is a steady decrease in the driving buoyant force. There

are two approaches to minimizing the effect of the energy accumulation. One method is to carefully choose geometry that decouples the condition of the storage volume from the strength of the buoyant force. Another method is to accept the variance in driving pressure, but implement frictional loss behavior that minimizes its effect on the volumetric flow rate.

Before attempting to optimize the transient performance of the thermosyphon, the system must be designed to meet the desired flow rate and temperature rise at the beginning of the charge cycle. With this objective in mind, two alternative temperature profiles that are appropriate at the beginning of the charge process are considered. The simplest approach assumes that the storage volume is entirely uncharged ($T = 0$) and that the riser is uniformly heated to the setpoint temperature ($T = 1$). A more realistic temperature profile assumes an uncharged storage volume, but with a more realistic temperature profile in the riser. The more realistic riser temperature profile is the initial temperature at the inlet to the heating section with a linear variation to the setpoint temperature at the heater outlet, with the remaining portion of the riser assumed to be at the setpoint. Both of these methods are developed and compared to each other in the following paragraphs. Recognizing that these methods only serve to approach the desired temperature rise at the beginning of the charge cycle, an attempt to predict or improve the transient performance as energy accumulates in the storage volume must follow.

Considering first the simpler case, a uniform riser temperature, an energy balance applied to the heating section gives simply

$$\hat{\dot{W}}_e = \rho c_p \hat{\dot{V}} (\hat{T} - \hat{T}_o), \tag{15}$$

where $\hat{T} - \hat{T}_o$ is taken to be the temperature rise across the heating section. Dividing both sides by $\rho c_p \hat{\dot{V}}_o \Delta \hat{T}_{sp}$ reduces the result to the dimensionless expression,

$$T = \frac{1}{\dot{V}}. \tag{16}$$

Substituting this result into the quasi-steady form of the dimensionless momentum equation leads to the result

$$\Gamma\lambda(Re)\dot{V}^2 = \int_0^1 \frac{1}{\dot{V}}\,ds. \tag{17}$$

The desired operating point is that which yields the characteristic velocity ($\dot{V} = 1$), which in turn produces the specified temperature rise ($T = 1$). The obvious result is to select the flow restriction such that

$$\Gamma\lambda(Re_o) = 1. \tag{18}$$

Figure 3 shows the result of a simulation with parameters chosen using the guidance of Equation (18). The simulation spans the time required to circulate one storage volume through the flow loop. The volumetric flow rate begins near unity, representing the characteristic flow rate, however it is observed to decay as the simulation progresses through time and energy accumulates in the system. The dimensionless time required to circulate one storage volume is greater than unity as a result of the actual volumetric flow rate decaying below the characteristic flow rate. Figure 3 also shows the predicted temperature as a function of the dimensionless time at the riser outlet and at five evenly spaced vertical locations within the storage volume. The temperature of the fluid leaving the riser is shown to increase in response to the decaying flow rate. The traces of the storage volume temperature indicate a stratified storage volume, although the temperatures increase with time due to the rising temperature of the fluid displacing the stored volume.

The simplistic temperature profile used to develop Equation (18) is an approximation that will obviously improve as the relative heating length decreases. A better representation of the temperature within the heating section is easily attainable. Beginning from a steady state energy balance on a differential element of the heating section and then integrating from the inlet to position s within the heating section yields the expression,

$$\hat{\dot{W}}_e' \cdot \hat{s} = \rho \hat{\dot{V}} c \left(\hat{T}(\hat{s}) - \hat{T}_o \right) \tag{19}$$

Dividing by the equality $\hat{\dot{W}}_e' \hat{l}_h = \rho \hat{\dot{V}} c \Delta \hat{T}_{sp}$ yields the dimensionless expression,

$$T(s) = \frac{s}{l_h} \frac{1}{\dot{V}}, \tag{20}$$

applicable for $0 \leq s \leq l_h$. Using this expression for temperature in the heating section and assuming that the temperature of the remainder of the riser is the same as the heater outlet, the steady momentum equation becomes

$$\Gamma \lambda(Re) \dot{V}^2 = \int_0^{l_h} \frac{s ds}{l_h \dot{V}} + \int_{l_h}^1 \frac{ds}{\dot{V}}. \tag{21}$$

Again, the desired design point is that which produces the characteristic flow rate, $\dot{V} \equiv 1$. The result is therefore a flow restriction satisfying

$$\Gamma \lambda(Re_o) = 1 - \frac{l_h}{2}. \tag{22}$$

Although this result is very similar to Equation (18), there are benefits to incorporating the added complexity. In addition to more accurately representing the physical situation, this approach explicitly introduces the heating length parameter, l_h. Incorporating l_h into Equation (22) provides one indication of the affect changing the heating length has on the system and is in line with physical expectation. The strength of the buoyant force decreases as the length of the heating section increases. As anticipated, the slightly more involved expression collapses to the simpler version as the heating length approaches zero.

The affect of variations in the parameter Γ is shown in Figure 4, where the outlet temperature of the heating section is plotted against time. The multiple curves on this figure represent thermosyphon designs with different values of the product $\Gamma \lambda(Re_o)$. Included among these designs are the two guided by the preceding design points $\Gamma \lambda(Re_o) = 1$ and $\Gamma \lambda(Re_o) = 1 - l_h/2$. As expected, the riser outlet temperature just after startup is closest

to the setpoint temperature when $\Gamma\lambda(Re_o)$ is chosen to be $1 - l_h/2$, however choosing the product $\Gamma\lambda(Re_o)$ to be unity is likely an acceptable approximation.

In the present investigation, desirable performance refers to the system's ability to evenly heat the storage component to the setpoint temperature. Figure 4 shows the riser outlet temperature as a function of time and therefore provides an indication of the thermosyphon performance. A more direct illustration of the system capability is given by the riser outlet temperature plotted versus the fraction of the storage volume that has been circulated through the thermosyphon loop. The difference between these two perspectives can be emphasized by considering the relationship between dimensionless time and the fraction of the storage volume circulated. In dimensional terms the volume of fluid circulated through the loop is the time integral of the volumetric flow rate, $\hat{V} = \int \dot{\hat{V}} dt$. The fraction of the storage volume circulated is clearly more relevant than the dimensional volume, therefore the dimensionless volume fraction is introduced as $V_f = \hat{V}/\hat{V}_s$ and is computed from $V_f = \int \dot{V}(t) dt$. From this viewpoint, the relationship between dimensionless time and volume fraction is linear when the volumetric flow rate is constant. In such a situation the shape of the outlet temperature profile would appear the same whether plotted versus the dimensionless time or the volume fraction. The volumetric flow rate is not constant in the thermosyphon system however, and as a result, the relationship between the dimensionless time and the volume fraction is nonlinear. A plot of the riser outlet temperature versus the volume fraction is given in Figure 5.

The most significant result of the results shown in Figure 5 is not the temperature of the fluid exiting the heater at the beginning of the charge cycle, but instead the shape of the transient temperature profile. The simulations indicate that the parameter Γ has only a very small impact on the shape of the outlet temperature profile when plotted versus the volume fraction. In essence, the parameters embedded in Γ cause only a bias shift in the temperature profile. This outcome is most unforeseen when considering the extent to which the thermosyphon design is embedded within this single parameter. Among the parameters

included in Γ are the overall size and proportions of the system, the rate of heat input, as well as the dimensions of the restriction section. In part this is a positive outcome, because it reveals that a system can be easily scaled to larger or smaller physical sizes and the setpoint adjusted without affecting the overall performance of the storage device. However, this result offers no suggestions pertaining to possible improvements in the uniformity of the charge profile and therefore performance.

3.2 Flow Regime Analysis

Two general approaches for improving the transient performance of the present thermosyphon based system have already been suggested. One strategy is to choose geometry that minimizes the variation in pumping power over the course of the charge cycle. Another method is to utilize frictional loss behavior that minimizes the affect this variation has on the volumetric flow rate. We have already shown that many of the parameters pertinent to the thermosyphon design have no effect on either of these two aspects. The numerous parameters embedded in the term Γ only offset the temperature profile, achieving no improvement in the shape of the riser outlet temperature profile.

The functional relationship between the frictional loss coefficient and the Reynolds number in the restriction is one characteristic of the thermosyphon that can influence the transient performance. The nature of this relationship is determined by the type of flow regime that is present in the restriction. The functional dependance can vary from being inversely proportional to the Reynolds number in one regime, to being directly proportional in another. The impact of the transient pumping power on the volumetric flow rate can therefore potentially be reduced by carefully designing the system to operate within a specific flow regime. The most favorable performance is expected from a flow regime where the frictional loss increases most strongly with flow rate. In such a situation, a smaller change in the volumetric flow rate is necessary to balance the unavoidable change in the driving pressure during the charge cycle.

The suggestion that performance can be affected by the choice of flow regime seems to be a contradiction to the earlier conclusion that the parameters grouped within Γ do not have an influence on the transient performance. The discrepancy is that it is the *target* Reynolds number, Re_o, which is embedded within Γ. The previous discussion confined the functional dependence of λ to a single flow regime. Assuming that the flow regime is not affected by the observed change in the Reynolds number, the previous statements are accurate. The affect of alterations in the flow regime is the topic of the forthcoming discussion.

The group of terms in the governing momentum equation that relate to the relative frictional loss serve as a starting point for investigation into the effect of flow regime on the transient performance. From equation (7) this group of terms is $\Gamma\lambda(Re)\dot{V}^2$. Substituting for the loss coefficient using the general form $\lambda = a/Re^b + c$ and substituting for the Reynolds number using $Re = \dot{V}Re_o$, this part of the momentum equation expands into

$$\Gamma\dot{V}^2\lambda = \Gamma\dot{V}^2\left[\frac{a}{(\dot{V}Re_o)^b} + c\right]. \tag{23}$$

The frictional losses are proportional to $\dot{V}^{2-b}$ if the contribution of the term c is negligible. According to the argument already given it is desirable for the flow resistance to have a high dependance on the volumetric flow rate. For this reason, the most desirable flow regime is one where the loss coefficient λ is well represented by the form $\lambda = a/Re^b$ and where the coefficient b is small, preferably less than one.

In an effort to identify the flow regime that will physically achieve the most favorable results, a range of Reynolds numbers is considered which spans the four distinct flow regimes. Appropriate functions representing the loss coefficient for each regime are identified. For low Reynolds numbers extending up to 2300 the flow is considered laminar and the familiar Fanning friction factor result applies, $\lambda = 16/Re$. The transition regime extends from Reynolds numbers beginning at approximately 2300 and ending at approximately

4000. The loss coefficient for this type of flow is

$$\lambda = \frac{2.3 \times 10^{-8}}{Re^{-3/2}} + 0.0054, \tag{24}$$

as given by Bhatti and Shah [24]. If the flow passage is considered hydraulically smooth and the Reynolds number is greater than 4000 the flow is considered turbulent and the loss coefficient is given by the Blasius relation [25]

$$\lambda = \frac{0.0791}{Re^{1/4}}. \tag{25}$$

Finally, if the Reynolds number is greater than 4000 and the flow passage is sufficiently rough the flow is considered highly turbulent and the loss coefficient is taken to be a constant, $\lambda = c$. It is noteworthy that although the development has implied that the frictional losses are due to major losses, minor losses are also readily accommodated. Flow resistance due to geometry such as contractions and entrances has the same functional behavior as highly turbulent flow where the loss coefficient is a constant.

Among the flow regimes that have been identified, transitional flow is expected to produce the most desirable performance. The magnitude of the loss coefficient for this type of flow increases with the Reynolds number ($b = -3/2$), whereas it is decreasing or constant for the other regimes. Figure 6 illustrates the influence that the frictional loss behavior has on the transient performance. This figure shows the results of simulations corresponding to all four flow regimes. For each simulation the transient temperature exiting the heating section is given over the time of one charge cycle. The results confirm the expectation that performance improves as the coefficient b decreases.

3.3 Analysis of Buoyant Force

The variation in the driving buoyant force as a result of energy accumulation is the fundamental difficulty in achieving desired performance with the thermosyphon system

being considered. Tailoring the loss behavior has shown some improvement in performance, however the most direct approach is to simply eliminate the change in pumping power. Mathematically the driving force is represented in the momentum balance as the integral of temperature around the loop. In the steady momentum equation this force is balanced by the frictional losses, therefore

$$\Gamma \lambda \dot{V}^2 = \int_0^2 T(s)G(s)ds. \tag{26}$$

The integral of temperature can be divided into two parts. One part pertains to the riser section, where an increase in temperature contributes to higher driving pressure ($G(s) = 1$). The other part of the temperature integral relates to the downcomer, where an increase in temperature reduces the driving pressure ($G(s) = -1$). Dividing the integral to reflect these two components, the momentum balance becomes

$$\Gamma \lambda \dot{V}^2 = \int_0^1 T(s)ds - \int_1^2 T(s)ds. \tag{27}$$

The fundamental difficulty is embodied in the second integral term, which represents the contribution of the downcomer. For the geometry considered, the thermal storage vessel constitutes the entire downcomer and as a result, the value of the corresponding integral term continuously increases as energy accumulates. The driving potential for flow around the loop therefore decays, since the riser temperature distribution changes less significantly. Several possibilities exist which could mitigate this behavior. These include changing the heater length, modulating the power input, and changing downcomer configuration.

Decreasing heater length would increase the first integral thereby lessening the impact of changes in the downcomer. More specifically, an increase in riser temperature has the greatest impact when the relatively high heater outlet temperature is achieved over as much of the riser as possible. This is achieved by minimizing the heating length and increasing the power density. The expectation that performance is improved as the heating length is

decreased is supported by the results shown in Figure 7. The graphs of dimensionless riser outlet temperature show that a more uniform temperature profile is obtained as the heating length decreases. A second possibility for improving the temperature profile would be modulating the power input. While a relatively simple controller would likely be adequate, the consequence would be a reduction in the energy transfer to the system and diminished performance. A final possibility would be changing the configuration of the downcomer to reduce the affect of energy accumulation on driving pressure. This could be achieved by relaxing the requirement that the storage vessel must extend the entire downcomer. Such a solution, while effective, would not allow the thermosyphon system to fit within the confines of the thermal storage vessel.

3.4 Startup Transient

Our attention to this point has focused on the time scale of one complete charge cycle. The preceding traces of riser outlet temperature condense the small time behavior of the startup transient to a narrow and unrecognizable portion of the figures. The dynamics of the startup transient have been further de-emphasized by neglecting the inertia in the proposed design for the restriction geometry. The method used to choose the geometry of the restriction implies that the design point is instantaneously achieved at startup, even though this is physically unrealistic. The startup transient is relevant however, particularly in regards to overshoot of the setpoint and the time response of the system.

The nature of the small time scale behavior is dominated by the system's inertia. This is quantified by the coefficient of the unsteady term in the momentum balance. In dimensionless form this coefficient has been symbolized as

$$\frac{R_s^2 Re_o^2}{Gr} \int_0^2 \left(\frac{D_r}{D} \right)^2 ds. \tag{28}$$

The integral in this group of terms embodies the variation in dimensionless diameter, $D = D(s)$ and is referred to as the geometry ratio. However, since the flow restriction section has

the smallest diameter its value is approximately one. With this assumption, the coefficient simplifies to $R_s^2 Re_o^2/Gr$. Since the preferred flow behavior is in the transition regime, the nominal Reynolds number is fixed at the highest end of this regime, $Re_o \sim 4000$. Since the Grashoff number is indirectly specified by the aspect ratio, the aspect ratio is the single unconstrained parameter that affects the system inertia. Reasonable values for the aspect ratio range from one to five, where a typical value for a domestic hot water heater is approximately 3.25. Simulations indicate that there is very little change in the small time scale behavior due to variations of the aspect ratio within this range. A plot showing the riser outlet temperature and the volumetric flow rate during the initial transient is given by Figure 8 with an aspect ratio of 3.25. The variation is representative however, of the relevant range of aspect ratios.

The volumetric flow rate of the simulation illustrated by Figure 8 indicates that the system is operating below the characteristic flow rate during the startup transient. This is the anticipated affect of the system's inertia. Further, it is apparent that there is a time delay from the moment when heat addition begins to occur ($t = 0$) to the time when the signal is detected at the riser outlet. This is a result of the time required for the "packet" of fluid to be heated in the lower portion of the riser and to travel to the riser outlet. The illustration indicates that the delay is approximately 0.004 units dimensionless time or approximately 24 seconds for a 40.0 gallon vessel of water with a desired temperature increase of $42.8^{\circ}C$ using 4.5 kW of power. By comparison, the transit time along the length of the riser tube predicted by flow at the nominal volumetric rate is approximately 17 seconds for the same system.

4. SUMMARY AND CONCLUSIONS

A closed loop thermosyphon which is allowed to accumulate significant thermal energy exhibits behavior markedly distinct from that of a system with a balanced heat load. In the unbalanced situation, the system is inherently transient and a steady state

solution does not exist. The driving pressure which circulates the working fluid through the heating portion of the loop decreases as the system accumulates energy in the storage component. Confined to a fixed heat input, the temperature of the fluid leaving the heat input section and delivered to the storage component continuously increases in response to the decaying driving pressure. The result is that the vertical variation of the storage temperature, referred to as the charge profile, is less than uniform. Using appropriate dimensional scales the governing conservation equations have been made dimensionless and the parameters affecting the uniformity of the charge profile have been identified in an effort to improve the performance.

Interestingly, many of the parameters describing the system have no influence on the shape of the charge profile. The parameters embedded in the term we have identified as Γ only shift the charge profile causing a change in the absolute temperatures, while the shape of the profile is virtually unaffected. Among the quantities embedded in Γ are the aspect ratio of the tank, the rate of heat input, as well as the relative length and diameter of the portion of the loop dominating the frictional loss.

The flow regime in the flow restriction was found to influence the shape of the charge profile. The most favorable results were obtained when the frictional loss increased with the volumetric flow rate. This is achieved when the primary flow restriction operates in the transitional regime. While the frictional loss was confined to one section of the loop in the present analysis in order to isolate this factor, a more realistic approach could include frictional loss from all portions of the loop. The real system could nevertheless be designed to allow the losses in one portion of the loop to be dominant and operating in the transitional regime.

The length of the heating portion of the loop is the other aspect of the thermosyphon that was found to influence the shape of the charge profile. It was shown that the most favorable performance is achieved by increasing the power density and reducing the relative length of the loop where heat addition occurs.

While the dimensionless analysis provides insight into the thermosyphon design that is not specific to a particular scale, application of the design to a physical system is straightforward. One approach is to begin by specifying the desired dimensional temperature rise and available rate of heat input. The scale of the volumetric flow rate then follows. Having quantified the nominal flow rate, and with selection of a target flow regime and Reynolds number, the hydraulic diameter of the portions of the loop where frictional losses are dominant can be chosen. The results have shown that the steady form of the momentum equation can be solved with an approximate temperature distribution appropriate to just after startup. Based on this approximation, the required length of the dominant loss components can be determined, thereby throttling the flow to achieve the desired setpoint. Selection of the storage volume size and aspect ratio allows the remaining dimensional quantities to be readily computed.

Nomenclature

Dimensional quantities are denoted by a hat, *eg* $\hat{t}$.

Roman

A	cross sectional area
c_p	specific heat
D_h	hydraulic diameter
F	binary frictional loss function
G	flow path orientation
g	acceleration due to gravity
Gr	Grashoff number, see equation (9)

H overall system height

J binary heat input function

k thermal conductivity

l length

Pe Peclet number, see equation (14)

R_s aspect ratio

Re Reynolds number

s position

T temperature

t time

V volume

v flow velocity

$\dot{V}$ volumetric flow rate

$\dot{W}_e$ energy transfer rate

$\dot{W}_e'$ rate of electric heat input per unit length

Greek

α thermal diffusivity

β coefficient of thermal expansion

Γ ratio between buoyant and frictional forces, see equation (11)

λ frictional loss coefficient

ν kinematic viscosity

ρ density

τ_w wall shear stress

Subscripts and Superscripts

f fraction

h heating

o design point or nominal condition

r restriction

s storage

sp set point

References

1. R. Greif, Natural circulation loops, ASME J. Heat Transfer, vol. 110, pp. 1243–1258, 1988.

2. B. Gebhart, Y. Jaluria, and R. L. M. B. Sammakia, Buoyancy-induced flows and transport, Hemisphere Publishing Corporation, 1988.

3. K. E. Torrance, Open-loop thermosyphons with geological applications, ASME J. Heat Transfer, vol. 101, pp. 677–683, 1979.

4. K. E. Torrance and V. W. C. Chan, Heat transfer by a free convection loop embedded in a heat-conducting solid, Int. J. Heat Mass Transfer, vol. 23, pp. 1091–1097, 1980.

5. H. H. Bau and K. E. Torrance, On the stability and flow reversal of an asymmetrically heated open convection loop, Journal of Fluid Mechanics, vol. 106, pp. 417–433, 1981.

6. H. F. Creveling, J. F. D. Paz, J. Y. Baladi, and R. J. Schoenhals, Stability characteristics of a single-phase free convection looplity characteristics of a single-phase free convection loop, Journal of Fluid Mechanics, vol. 67, pp. 65–84, 1975.

7. R. Greif, Y. Zvirin, and A. Mertol, The transient and stability behavior of a natural convection loop, ASME J. Heat Transfer, vol. 101, pp. 684–688, 1979.

8. P. S. Damerell and R. J. Schoenhals, Flow in a toroidal thermosyphon with angular displacement of heated and cooled sections, ASME J. Heat Transfer, vol. 101, pp. 672–676, 1979.

9. M. Sen, E. Ramos, and C. Trevino, The toroidal thermosyphon with known heat flux, Int. J. Heat Mass Transfer, vol. 28, pp. 219–233, 1985.

10. P. K. Yuen and H. H. Bau, Optimal and adaptive control of chaotic convection - theory and experiments, Physics of Fluids, vol. 11, pp. 1435–1448, 1999.

11. G. Muscato and M. Xibilia, Modeling and control of a natural circulation loop, Journal of Process Control, vol. 13, pp. 239–251, 2003.

12. T. N. Swift, J. A. Miller, and D. C. Hittle, A systematic approach to improving thermosyphon sdhw model performance, in Solar Engineering 1996, Proceedings of ASME Solar Energy Division Conference, pp. 165–171, 1996.

13. J. D. Burch and K. M. Gawlik, Using an ersatz thermosiphon loop to model natural convection flows inside a shallow enclosure, in Proceedings of Solar 2001, pp. 183–190, 2001.

14. A. Mertol, W. Place, T. Webster, and R. Greif, Detailed loop model analysis of liquid solar thermosyphons with heat exchangers, Solar Energy, vol. 27, pp. 367–386, 1981.

15. S. D. Dahl and J. H. Davidson, Mixed convection heat transfer and pressure drop correlations for tube-in-shell thermosyphon heat exchangers with uniform heat flux, ASME J. Solar Energy Engineering, vol. 120, pp. 260–269, 1998.

16. S. D. Dahl and J. H. Davidson, Applicability of uniform heat flux nusselt number correlations to thermosyphon heat exchangers for solar water heaters, ASME J. Solar Energy Engineering, vol. 121, pp. 85–90, 1999.

17. G. L. Morrison and J. E. Braun, System modeling and operation characteristics of thermosyphon solar water heaters, Solar Energy, vol. 34, pp. 389–405, 1985.

18. Y. Zvirin, A. Shitzer, and A. Bartal-Bornstein, On the stability of the natural circulation solar heater, in International Heat Transfer Conference, vol. 2, pp. 141–151, Hemisphere Publishing Corp., 1978.

19. K. O. Homan, Thermodynamic optimization of system configuration for electric water heating with storage: fully-mixed store, in Proceedings of the ASME Advanced Energy Systems Division, pp. 479–491, 2001.

20. J. W. McMenamy and K. O. Homan, Transient and rate-dependent performance of conventional electric storage water heating systems, ASME J. Solar Energy Engineering, vol. 128, pp. 90–97, 2006.

21. J. W. McMenamy, Transient and rate dependent performance of conventional and thermosyphon-based electric storage water heating systems, Master's thesis, University of Missouri-Rolla, 2004.

22. P. Ranganathan, Z. Vafa, R. Schoenhals, and F. Gilleland, An experimental and analytical study of a thermosiphon-type thermal energy storage system, in Proceedings of The Seventh International Heat Transfer Conference, vol. 6, pp. 479–484, 1982.

23. B. van Leer, Towards the ultimate conservative difference scheme. iv. a new approach to numerical convection, Journal of Computational Physics, vol. 23, pp. 276–299, 1977.

24. M. S. Bhatti and R. K. Shah, Handbok of Single-Phase Convective Heat Transfer, John Wiley & Sons, 1987.

25. H. Schlichting, Boundary Layer Theory, McGraw-Hill, 1987, seventh ed.

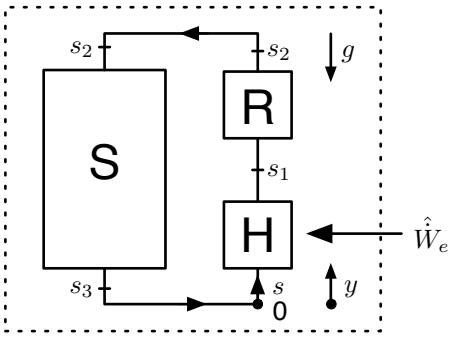

Figure 1 Conceptual schematic of the thermosyphon configuration with “S” designating the storage volume, “H” the heat input component, and “R” the flow restriction.

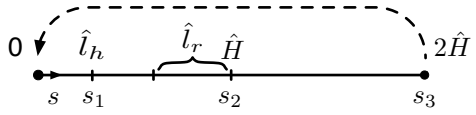

Figure 2 Schematic of the quasi one-dimensional thermosyphon model.

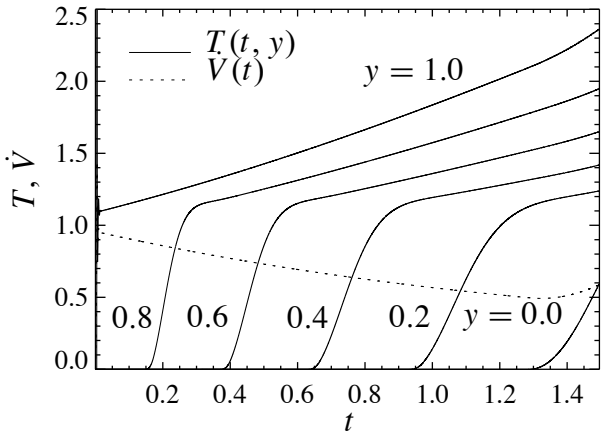

Figure 3 Traces of volumetric flow rate and temperature in the storage volume as a function of time. Temperature is given for the riser outlet and at five evenly spaced vertical locations within the storage volume. $y = 0.0$ represents the location at the bottom of the storage. $y = 1.0$ is the riser outlet temperature and also the temperature in the upper most portion of the storage. For this simulation $\Gamma\lambda(Re_o) = 1$.

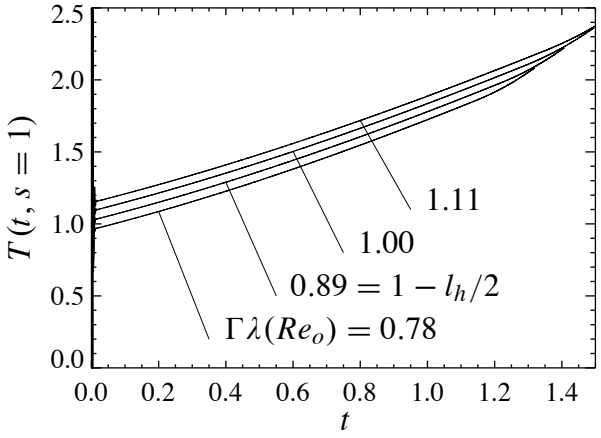

Figure 4 Variation of riser section outlet temperature, $T(t, s = 1)$, as a function of time for a range of the dimensionless loss parameter, $\Gamma\lambda(Re_o)$.

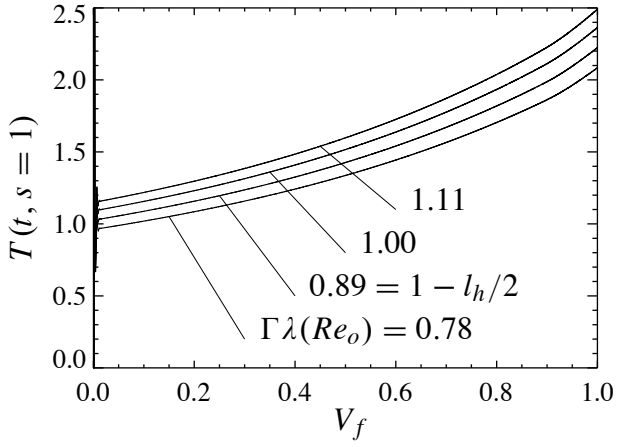

Figure 5 Riser section outlet temperature versus volume fraction for variations of the flow loss parameter $\Gamma\lambda(Re_o)$.

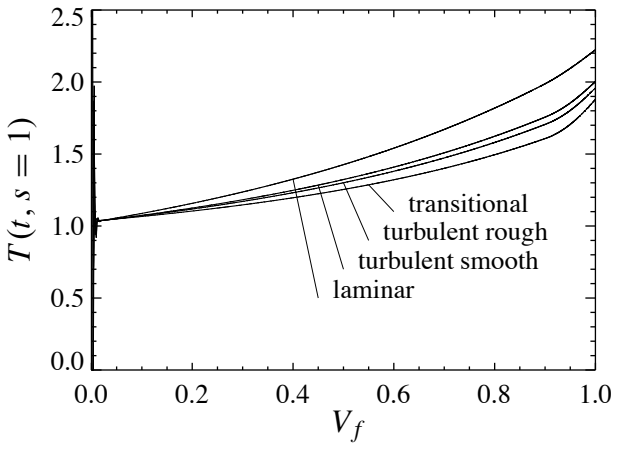

Figure 6 Variation of riser outlet temperature with volume fraction for four distinct flow regimes: laminar, transitional, turbulent smooth, and turbulent fully rough regimes. For these simulations $\Gamma\lambda(Re_o) = 1 - l_h/2$.

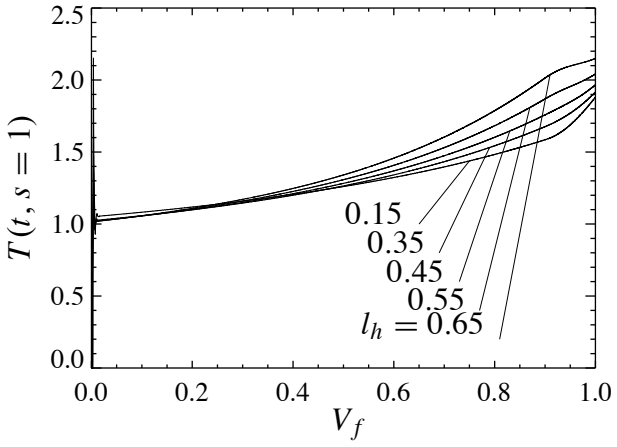

Figure 7 Variation of riser outlet temperature with heating length. More desirable performance is obtained as the heating length is reduced. For these simulations $\Gamma\lambda(Re_o) = 1 - l_h/2$.

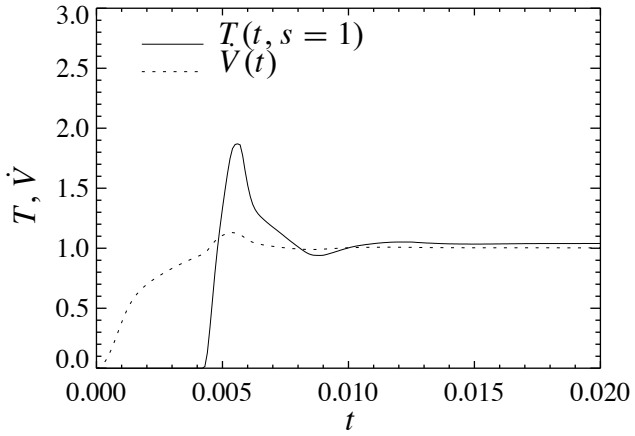

Figure 8 Traces of riser outlet temperature and volumetric flow rate during startup transient for $R_s = 3.25$. $\Gamma\lambda(Re_o)$ is selected to be $1 - l_h/2$.

2. Advanced Thermal Storage Incorporating an Integrated Thermosyphon and Constant Temperature Heat Addition*

K. S. Benne and K. O. Homan†
Department of Mechanical & Aerospace Engineering
University of Missouri-Rolla, Rolla, Missouri 65409–0050
Tel: 573–341–6622, Fax: 573–341–4115
Email: khoman@umr.edu

Abbreviated Title: Advanced Thermal Storage.

*Submitted to *Numerical Heat Transfer, Part A Applications*, (Version 7).
†Author to whom correspondence should be addressed

Abstract

A unique thermal storage device incorporating an integrated thermosyphon is analyzed numerically. Energy is added from a constant temperature heat source situated within one portion of the thermosyphon loop. A comparison is made between the stratified thermosyphon device and a fully mixed storage volume with constant temperature heat addition and it is determined that a higher rate of energy transfer is possible for the thermosyphon device. The fundamental challenge is that as energy accumulates within the thermosyphon storage volume, the driving buoyant force and volumetric flow rate decay, causing less than optimal power delivery. The results of this study indicate that the undesirable consequence of energy accumulation can be minimized by targeting the dominant frictional losses to the transitional regime.

1. INTRODUCTION

A thermosyphon is a flow loop that circulates fluid using the buoyancy generated by a temperature gradient instead of a conventional pump. Thermosyphons have been applied to a variety of applications, however they are particularly well suited for applications where energy efficiency, cost, and reliability are important [1]. A few of these applications are solar domestic hot water (SDHW) systems, geothermal energy systems, and the cooling system of a nuclear reactor.

The present study pertains to a thermosyphon loop that is integrated within a conventional thermal storage device, such as a domestic hot water (DHW) system. During heat addition, this unique configuration maintains stratification by isolating the rising plume of heated fluid from the main storage volume [2]. Driven by natural convection, cold fluid is drawn from the lower portion of the storage volume, heated, and returned to the top of the storage volume, thereby eliminating large scale thermal mixing. Because the quality of the added energy is preserved, fluid exiting the thermosyphon riser can be readily utilized

[3]. In the event of a draw, the thermosyphon storage device can make use of fluid energy accumulated in the storage vessel in addition to fluid energy exiting the thermosyphon riser. Conceptually, the two energy streams act in parallel creating a hybrid system where the benefits of a conventional storage device and an instantaneous heater are obtained simultaneously. The present study specifically focuses on the energy addition or charge process of the storage volume. Heat is added by a constant temperature source simulating the condensing heat exchanger of a vapor compression heat pump.

There is a large body of literature pertaining to thermosyphon flow loops. Typically this work is divided between open and closed loop thermosyphons [4]. In the open configuration fluid is transported between large reservoirs of fluid by means of one or more connecting ducts where heat is added or removed. Investigations on this type of system have been carried out on the basis that the reservoirs are effectively of infinite size with a state independent of the thermosyphon loop [5, 6, 7]. A variety of studies have also been carried out pertaining to the closed loop thermosyphon. In this configuration, fluid is continuously circulated around a closed path with alternating heating and cooling sections. The dynamics of the startup transient and the stability characteristics have been thoroughly investigated for the closed loop [8, 9, 10, 11, 12, 13].

The thermosyphon storage device of the present study is markedly distinct, however, from the work cited, because the dynamics of the thermosyphon and the condition of the thermal reservoir are coupled. Unlike the open thermosyphon, the thermal reservoir is finite and coupled with the thermosyphon loop. The present device also differs from the closed loop thermosyphon, because heat is accumulated in the system instead of being alternately added and removed. Very simply, the base steady state solution used in the preceding studies does not apply to the configuration being considered. The body of work pertaining to thermosyphon SDHW is more relevant. These studies can be categorized as direct and indirect systems. The indirect configuration isolates the thermosyphon loop from the main storage volume using a heat exchanger. Numerous studies pertaining to the indirect system

are reported in the literature [14, 15, 16]. More similar to the present configuration, the direct SDHW system has the thermal storage integrated within the flow path. Literature pertaining to the direct SDHW system is also available [17, 18]. Both configurations are relevant to the present investigation, because the thermosyphon is in communication with a finite thermal reservoir, and during daytime charging, the thermosyphon SDHW system accumulates energy within a storage component. Key differences however are that the solar irradiation varies in time, the heat input is a time varying temperature boundary instead of a constant temperature boundary, and the heat transfer area (solar collector) is external to the storage volume and can be positioned in a vertical position below the storage volume.

Additional research applicable to the present configuration has been carried out by [19]. Here a thermal storage volume with an electric resistance side arm heating loop is investigated. This study is especially similar to the present work, because the thermosyphon is vertically confined within the storage height. One observation made by this work is that the volumetric flow rate significantly decays as the storage volume accumulates energy. Because the flow rate through the heating section is variable, the heated storage temperature is not uniform.

The motivation behind the present study has two components. In part this study is driven by the recognition that heat transfer can be improved for a stratified system, because a larger temperature differential can be sustained between the heat source and the working fluid [20, 21]. Secondly, this study is based on the recognition that energy accumulation in the storage volume causes an unwanted decrease in the strength of the driving buoyant force and consequentially a decrease in the volumetric flow rate. In a related paper we showed that for a similar thermosyphon configuration with constant heat addition, the decay in flow rate results in rising temperature exiting the heating portion of the thermosyphon and ultimately a less than uniform charge profile [22]. It was found that the charge profile can be improved by targeting the frictional loss behavior to the transitional flow regime and by reducing the relative height of the heating portion of the thermosyphon loop. For the

present configuration with a constant temperature heat source, obtaining a uniform charge profile is less problematic, however the inherent decay in volumetric flow rate now causes a decrease in the power delivered to the storage volume. Despite this difficulty, we will show that the thermosyphon storage device can maintain higher power delivery over the course of the charge cycle compared to a heat exchanger immersed in a fully mixed storage volume. We will also show that power delivery can be improved by the choice of flow regime.

2. PROBLEM FORMULATION

2.1 Problem Description

A thermosyphon loop with three distinct sections is the basis of the conceptual model used in this study. They are a heat addition section, a restriction section, and a storage volume. Figure 1 identifies the arrangement of these sections. The heat addition and restriction sections form the riser of the thermosyphon, while the downcomer is composed entirely of the storage volume. Gravity is everywhere acting downward as indicated by the illustration. Fluid is drawn from the bottom of the storage vessel into the heating section. The heated fluid then travels up, due its buoyancy, through the restriction section and delivered to the top of the storage volume. The system is adiabatic except for the designated heating section. This arrangement represents the thermal charge process where energy accumulates in the storage vessel. The storage vessel has a significantly larger cross sectional area compared to the other portions of the thermosyphon loop and this section accounts for most of the volume and stored energy in the system. Because the storage volume is stratified, a thermocline dividing the heated and unheated fluid travels down the storage volume as energy is accumulated. The flow restriction has the smallest cross sectional area of the flow loop and this section plays a critical role by throttling the volumetric flow rate through the thermosyphon loop. Frictional losses outside of the designated restriction section are neglected in an attempt to isolate the characteristics of a specific flow regime. After the

characteristics of a particular flow regime are understood using the simplified loop, a physical system can be designed to target the most desirable flow behavior.

A quasi one-dimensional model illustrated by Figure 2 is used to simulate the system just described. In this model there is a single spatial coordinate, s, representing the position around the loop. The coordinate begins at the entrance to the heating section and extends to the outlet of the storage volume where the loop is then closed. The cross sectional area of the flow path is a function of s. The overall height of the system, $\hat{H}$, is equivalent to the height of the storage tank. The heat input and restriction sections are vertically confined within the storage volume, however they may be physically positioned inside or outside of this component. In the present model only the vertical components are recognized, therefore the horizontal position of the components is irrelevant. The dimensional lengths of the heating and the restriction sections are $\hat{l}_h$ and $\hat{l}_r$ respectively. The length of the riser is equal to the overall system height, $\hat{H}$, but as indicated by Figure 2, may be less than the sum of $\hat{l}_h$ and $\hat{l}_r$. The heating section begins at the base of the riser and the restriction section ends at the outlet of the riser. The length separating these two components floats to allow the riser to extend the full height of the system. The total length of the flow loop is $2\hat{H}$.

2.2 Equation Development

The governing momentum balance is developed beginning from a differential element of the system and then integrating around the loop. The pressure and flux terms are continuous functions of the spatial coordinate and are eliminated by integrating around the closed path. In dimensional form, the momentum equation simplifies to

$$\left(\int \frac{d\hat{s}}{\hat{A}}\right) \frac{d\hat{\dot{V}}}{d\hat{t}} = -\int \frac{4\hat{\tau}_w}{\rho_o \hat{D}_h}\, d\hat{s} + g\beta \int \left(\hat{T} - \hat{T}_o\right) G(\hat{s}) d\hat{s}, \tag{1}$$

where $G(\hat{s})$ indicates the orientation of a particular section of the flow loop with respect to gravity. The value of $G(s)$ is taken to be positive one in the riser portion of the loop ($0 \leq \hat{s} < \hat{H}$) and negative one in the downcomer ($\hat{H} \leq \hat{s} < 2\hat{H}$). The dimensional

volumetric flow rate is denoted by $\hat{\dot{V}}$, the dimensional temperature by $\hat{T}$, and the initial temperature by $\hat{T}_o$. The dimensional cross-sectional area is symbolized by $\hat{A}$, however for the loss term the conventional hydraulic diameter, $\hat{D}_h$, is used. The cross-sectional area varies significantly with position, $\hat{A} = \hat{A}(\hat{s})$, while the volumetric flow rate varies only in time, $\hat{\dot{V}} = \hat{\dot{V}}(\hat{t})$, as dictated by conservation of mass. The temperature varies with space and time, $\hat{T} = \hat{T}(\hat{t}, \hat{s})$. The wall shear stress in the throttling section is defined as

$$\hat{\tau}_w = \frac{1}{2}\rho_o \hat{v}^2 \lambda, \tag{2}$$

where $\hat{v}$ is the local velocity and λ is the Fanning friction factor, a function of Reynolds number, $\lambda = \lambda(Re)$. The functional dependence of the friction coefficient on the Reynolds number is based on the fluid flow regime and is represented by the general form,

$$\lambda = \frac{a}{Re^b} + c. \tag{3}$$

The temperature profile within the flow loop is described by a one dimensional energy balance that includes the effects of diffusion due to conduction in the axial direction. Energy is added to the system only within the heating portion of the thermosyphon loop. The resulting differential energy equation is

$$\begin{aligned} \rho c_p \frac{\partial}{\partial \hat{t}}(\hat{A}\hat{T}) + \rho c_p \frac{\partial}{\partial \hat{s}}(\hat{A}\hat{v}\hat{T}) = \\ \frac{(U\hat{A}_h)}{\hat{l}_h}(\hat{T}_h - \hat{T}) \cdot J(s) + \frac{\partial}{\partial \hat{s}}\left(k\hat{A}\frac{\partial \hat{T}}{\partial \hat{s}}\right), \end{aligned} \tag{4}$$

where $J(s)$, similar to $G(s)$, is a binary function reflecting the portion of the loop over which heat is added. Within the heating section its value is one, elsewhere it is zero. The product $U\hat{A}_h$ represents the overall conductance of the condensing heat exchanger and $\hat{T}_h$ is the condensing temperature, presumed constant.

2.3 Non-dimensionalization

The dimensional form of the governing equations can be made more useful for the present application by choosing appropriate dimensional scales. The objective is to heat a fluid such as water from a starting temperature, $\hat{T}_o$, to a setpoint temperature, $\hat{T}_{sp}$. In pursuit of this goal the dimensionless temperature is defined according to $\hat{T} = \Delta\hat{T}_{sp}T + \hat{T}_o$, where $\Delta\hat{T}_{sp} = \hat{T}_{sp} - \hat{T}_o$. According to this selection the dimensionless temperature is initially zero and becomes unity at the setpoint. The time scale is chosen based on the time required to heat the storage volume from the initial temperature to the setpoint temperature at the desired heating rate. Symbolically, the dimensionless time is defined as,

$$t = \frac{\hat{t}}{\rho c_p \hat{V}_s \Delta\hat{T}_{sp}/\hat{\dot{Q}}_o}, \tag{5}$$

where $\hat{\dot{Q}}_o$ represents the nominal rate of heat transfer and $\hat{V}_s$ is the storage volume. The dimensional scale of the volumetric flow rate is chosen to be the flow rate required to circulate the entire storage volume during the time of one charge cycle. Using this scaling choice, the dimensionless volumetric flow rate is expressed as $\dot{V} \equiv \hat{\dot{V}}/\hat{\dot{V}}_o$ taking $\hat{\dot{V}}_o$ to be the nominal flow rate symbolized as

$$\hat{\dot{V}}_o = \frac{\hat{V}_s}{\rho c_p \hat{V}_s \Delta\hat{T}_{sp}/\hat{\dot{Q}}_o}. \tag{6}$$

Lengths are scaled by $\hat{H}$, which is the height of the storage volume and also the riser. The overall dimensionless length of the flow loop is two because of the chosen scale. The cross sectional area of the loop is scaled by the cross sectional area of the storage component.

Using the preceding choices to scale the variables in the governing momentum balance and identifying relevant parameter groups gives

$$\begin{aligned} &\frac{R_s^2 Re_o^2}{Gr}\left[\int_0^2 \left(\frac{D_r}{D}\right)^2 ds\right]\frac{d\dot{V}}{dt} = \\ &-2\frac{R_s^3 Re_o^2}{Gr}\left[\int_0^2 \frac{D_r^2}{D^5} F(s) ds\right]\lambda \dot{V}^2 + \int_0^2 G(s) T ds, \end{aligned} \tag{7}$$

where $s \equiv \hat{s}/\hat{H}$. The diameter of the cross section is denoted by D, where $D(s) \equiv \hat{D}(s)/\hat{D}_s$, and $\hat{D}_s$ is the diameter of the storage vessel. The nominal Reynolds number, Re_o, corresponds to the nominal flow rate moving through the restriction. Symbolically this is

$$Re_o = \frac{4\hat{\dot{V}}_o}{\pi \hat{D}_r \nu}, \tag{8}$$

where $\hat{D}_r$ is the dimensional diameter of the flow restriction section. The true Reynolds number at any instant in time is then given by $Re = \dot{V} Re_o$. The Grashoff number, Gr, is defined as

$$Gr = \frac{g\beta \Delta \hat{T}_{sp} \hat{H}^3}{\nu^2}. \tag{9}$$

The symbol R_s appearing in the momentum equation denotes the aspect ratio of the storage vessel and is defined as $R_s \equiv \hat{H}/\hat{D}_s$. The remaining symbol, $F(s)$, takes on a binary value of one in the flow restriction and zero elsewhere, effectively isolating the flow resistance to the restriction section. Assuming the frictional losses are confined to the restriction section, the momentum equation reduces to

$$\begin{aligned} &\frac{R_s^2 Re_o^2}{Gr}\left[\int_0^2 \left(\frac{D_r}{D}\right)^2 ds\right]\frac{d\dot{V}}{dt} = \\ &\qquad -\left(2\frac{R_s^3 Re_o^2 l_r}{Gr\, D_r^3}\right)\lambda \dot{V}^2 + \int_0^2 G(s) T ds, \end{aligned} \tag{10}$$

where $l_r \equiv \hat{l}_r/\hat{H}$, the dimensionless length of the flow resistance section. In an effort to condense the number of terms appearing in the final expression, the parameter Γ is defined

as,

$$\Gamma = 2 \frac{R_s^3 Re_o^2 l_r}{Gr\, D_r^3}. \tag{11}$$

Physically this parameter is the ratio between frictional flow resistance and driving buoyant force. Substituting, the final form of the momentum equation becomes

$$\frac{R_s^2 Re_o^2}{Gr} \left[\int_0^2 \left(\frac{D_r}{D} \right)^2 ds \right] \frac{d\dot{V}}{dt} = -\Gamma \lambda \dot{V}^2 + \int G(s) T\, ds. \tag{12}$$

The dimensions of the energy balance are scaled using the same scaling choices as the momentum equation. The dimensionless form of the energy equation is then

$$\begin{aligned} \frac{\partial T}{\partial t} + \frac{\dot{V}}{D^2} \frac{\partial T}{\partial s} = & - \frac{(U_o \hat{A}_h)}{\rho c_p \hat{\dot{V}}_o} \frac{U}{U_o} \frac{1}{l_h D^2} (T_h - T) J(s) \\ & + \frac{1}{Pe D^2} \frac{\partial}{\partial s} \left(D^2 \frac{\partial T}{\partial s} \right), \end{aligned} \tag{13}$$

where the nominal heating rate is taken to be $\hat{\dot{Q}}_o = \rho c_p \hat{\dot{V}}_o \Delta \hat{T}_{sp}$. The term U_o is the nominal overall heat transfer coefficient of the heat exchanger and the fraction U/U_o is the ratio between the actual heat transfer coefficient and the nominal value. Although, the ratio U/U_o will be taken to be unity, the formulation retains the possibility of a variable heat transfer coefficient. The Peclet number, Pe, is defined as

$$Pe = \frac{4 \hat{\dot{V}}_o \hat{H}}{\pi \hat{D}_s^2 \alpha}. \tag{14}$$

Defined in this way, the Peclet number reflects the ratio of diffusion time relative to advection time through the storage vessel at the nominal flow rate. The parameter group $(U_o \hat{A}_h)/\rho c_p \hat{\dot{V}}_o$ is recognized as the required NTU and for the present study symbolized as

NTU_o. Upon substitution, the energy equation becomes

$$\begin{aligned} \frac{\partial T}{\partial t} + \frac{\dot{V}}{D^2}\frac{\partial T}{\partial s} &= -\frac{NTU_o}{l_h D^2}\left(\frac{U}{U_o}\right)(T_h - T)J(s) \\ &\quad + \frac{1}{PeD^2}\frac{\partial}{\partial s}\left(D^2\frac{\partial T}{\partial s}\right). \end{aligned} \tag{15}$$

It is readily shown that, with present non-dimensionalization, the NTU_o is only a function of T_h, specifically

$$NTU_o = \ln\left(\frac{T_h}{T_h - 1}\right). \tag{16}$$

A plot of this function is given in Figure 3. Based on dimensional temperatures appropriate for a heat pump DHW system, a typical dimensionless high temperature is approximately 1.1 and the corresponding NTU_o is approximately 2.4.

2.4 Solution Method

The governing conservation equations are a coupled set composed of an ordinary differential equation and a partial differential equation. An analytical solution to this system of equations is not readily available. Previous work on similar problems has elected to either reduce the equations to a system of ordinary differential equations, or apply a finite difference approach. The present study adopts the latter technique.

The energy equation is solved with an implicit method using a central difference to approximate the diffusion term. The advection term of the energy equation is treated using a flux based approach, known as the monotonic piecewise linear (MPL) method [23]. This method provides second order accuracy for the advection term while avoiding the dispersion introduced by a central difference. The momentum equation is solved using the second order Adams Bashforth method with the buoyancy term lagged in time. In terms of numerical stability, the implicit method used to solve the energy equation avoids the timestep limitation otherwise imposed by the diffusion term, however the CFL condition still applies to the MPL and Adams Bashforth methods. This criteria significantly limits

the size of the timestep, because of the small diameter and high velocity in the restriction section. In spite of this fact, the numerical computation is relatively inexpensive and a more advanced method is not required.

3. RESULTS AND DISCUSSION

3.1 Fully Mixed System

A heat exchanger immersed in a fully mixed storage volume serves as an important point of comparison for the the thermosyphon system. A dimensional energy balance on the fully mixed system is,

$$\rho c_p \hat{V}_s \frac{d\hat{T}}{d\hat{t}} = (U\hat{A}_h)_m \cdot (\hat{T}_h - \hat{T}), \tag{17}$$

where $(U\hat{A}_h)_m$ distinguishes the UA product of the fully mixed system from the UA product of the thermosyphon system. In dimensionless terms, the energy balance for the fully mixed system becomes,

$$\frac{dT}{dt} = \frac{(UA)_m \Delta\hat{T}_{sp}}{\hat{\dot{Q}}_o}(T_h - T_o), \tag{18}$$

where T is the dimensionless storage temperature.

The scale of the heating power for the fully mixed energy balance must be carefully considered to ensure that a meaningful comparison is made between the fully mixed system and the thermosyphon system. In particular, due attention must be given to expression of the nominal heating rate, $\hat{\dot{Q}}_o$. For the thermosyphon system, $\hat{\dot{Q}}_o = \rho c_p \hat{\dot{V}}_o \Delta\hat{T}_{sp}$, the heat transfer rate giving the desired temperature rise, is certainly appropriate. However, scaling the fully mixed energy equation using this expression leads to the group of terms $(U_o\hat{A}_h)_m/\rho c_p \hat{\dot{V}}_o$. If the initial UA product for the fully mixed system, $(U_o\hat{A}_h)_m$, is equal to that of the thermosyphon system, $(U_o\hat{A}_h)$, the conclusion is that $(U_o\hat{A}_h)_m/\rho c_p \hat{\dot{V}}_o = NTU_o$, which is the ratio of the initial energy transfer rates. Thus, considering a value of NTU_o appropriate for the thermosyphon system, this scaling choice would allow the fully mixed

system at least twice as much heating power as the thermosyphon system. This is not satisfactory. In practice, the available heating power is limited by the size of the vapor compression system. In short, the choice of equal UA for each system does not provide a meaningful comparison.

A more meaningful comparison between the thermosyphon and fully mixed systems is one that provides the maximum heating power for both of the systems,

$$\hat{\dot{Q}}_o = \rho c_p \hat{\dot{V}}_o(\Delta \hat{T}_{sp}) = (U_o \hat{A}_h)_m(\hat{T}_h - \hat{T}_o). \tag{19}$$

Taking this heating power scale, the dimensionless form of the energy balance for the fully mixed system is

$$\frac{dT}{dt} = \binom{U}{U_o}_m \frac{(T_h - T)}{T_h}. \tag{20}$$

As for the thermosyphon system, the fraction $(U/U_o)_m$ is the ratio between the actual heat transfer coefficient and the nominal value. For simplicity, the ratio $(U/U_o)_m$ is taken as unity. Solving the differential equation for $T(t)$ leads to

$$T(t) = T_h \left(1 - e^{-\binom{U}{U_o}_m \frac{t}{T_h}}\right), \tag{21}$$

where $T(t)$ represents the temperature of the fully mixed storage volume at any instant during the charge cycle. An equally important quality of the fully mixed system is the power delivered to the storage fluid through the immersed heat exchanger. For the fully mixed system, the initial power delivery is a maximum at the beginning of the charge process by virtue of the high temperature differential, $\hat{T}_h - \hat{T}_o$. The temperature differential driving heat transfer decays as energy accumulates in the storage vessel. Quantitatively, the dimensionless power delivery at any instant during the charge process is

$$\dot{Q}_m(t) = \binom{U}{U_o}_m \cdot \frac{(T_h - T(t)}{T_h} = \binom{U}{U_o}_m e^{-\binom{U}{U_o}_m \frac{t}{T_h}}. \tag{22}$$

The dimensionless, cumulative energy added is simply

$$Q_m(t) = \int_0^t \dot{Q}_m(\tau)d\tau = T(t), \tag{23}$$

where $T(t)$ is given by Equation (21). Illustrations of the temperature and transient power of the fully mixed system are reserved for later discussion where they are compared to that of the thermosyphon system.

3.2 Charge Profile

Conventional heated thermal storage devices typically deliver fluid at the appropriate temperature by incorporating a high degree of internal thermal mixing and implementing a thermostat that is responsible for turning off the heat source when the desired temperature is met. The thermosyphon-based energy storage system which is the focus of the present study is essentially an instantaneous heater within a stratified storage device. One challenge for the thermosyphon system is that the riser outlet temperature, which becomes the stored fluid temperature, must be controlled either by modulating the heating power or by adjusting the volumetric flow rate. Modulating the power has an undesired thermal penalty, leaving the volumetric flow rate as the only suitable control. The flow restriction is the mechanism used to throttle the flow rate, therefore the desired temperature rise must be achieved by designing the restriction appropriately. Because the driving pressure is continuously decreasing as energy accumulates in the storage volume, the flow restriction necessary to achieve the nominal flow rate is variable during the charge cycle. Ideal behavior might be possible using an active throttling valve, however from a practical standpoint a passive solution is considerably more desirable.

The concerns related to achieving a uniform flow rate have already been thoroughly investigated for the case of constant heat addition [22]. In that work, the variation of the restriction design, embodied by $\Gamma\lambda(Re_o)$, was shown to effectively cause a bias shift in the volumetric flow rate and the riser outlet temperature profile when confined to a

specific flow regime. For the case of constant heat addition, the flow regime and the relative height of the heating section influence the shape of the temperature profile. For the present configuration, the riser outlet temperature is naturally limited by the temperature of the heat source. Although the flow rate diminishes, the temperature profile is bounded by the heating temperature. The parameter group $\Gamma\lambda(Re_o)$ should still be selected to produce the nominal volumetric flow rate and desired temperature rise (T=1) at the beginning of the charge cycle, however the outlet temperature profile will naturally be quite uniform, at least for low heating temperatures.

The product, $\Gamma\lambda(Re_o)$, is selected based on the quasi-steady form of the momentum equation along with suitable approximations for the temperature within the thermosyphon loop at the beginning of the charge cycle. The steady momentum equation is

$$\Gamma\lambda(Re)\dot{V}^2 = \int_0^2 G(s)T\,ds. \tag{24}$$

A rather coarse approximation is that at the beginning of the charge cycle the riser is evenly heated to the setpoint, $T = 1$, and the storage is completely uncharged, $T = 0$. Based on this assumption, the restriction geometry is chosen such that $\Gamma\lambda(Re_o) = 1$. A better approximation is to assume that the temperature linearly increases from zero to one within the heat addition section. This assumption leads to $\Gamma\lambda(Re_o) = 1 - l_h/2$. Either of these methods likely produce an *initial* temperature rise and volumetric flowrate that are sufficiently close to unity. The present investigation will use the more accurate version except for the occasion where the intent is to show the influence of $\Gamma\lambda(Re_o)$.

Figure 4 illustrates the behavior of the thermosyphon system with a heating temperature typical of heat pump water heating systems (HPWH), $T_h = 1.1$. The data is shown for the time necessary to circulate one storage volume at the actual volumetric flow rate. Traces of the storage volume temperature at several vertical locations show a stratified storage volume and a charge profile which is relatively uniform, remaining between 1 and 1.1,

except for very small time. The volumetric flow rate of the thermosyphon loop is also plotted to emphasize the fact that although the temperature profile is relatively uniform, the volumetric flow rate decays significantly. For comparison, the storage volume temperature of the fully mixed system during charging is overlaid on the thermosyphon data. It is clear from this comparison that the stratified thermosyphon system produces a portion of usable energy even from the beginning of the charge cycle, however usable energy is not available from the fully mixed system until the charge cycle is virtually complete.

For most HPWH systems, T_h of approximately 1.1 is appropriate. In broader context, it is also worthwhile to consider higher heating temperatures. As the temperature of the heat source is increased the temperature profile of the fluid exiting the thermosyphon riser becomes less favorable, viewed in terms of temperature uniformity. The parameters influencing the riser temperature profile also become emphasized as the temperature of the heat source is increased. Particularly, relative heating length, flow regime, and restriction design, $\Gamma\lambda(Re_o)$, become more significant. In this study, the influence of each of these parameters is considered individually and at multiple heating temperatures. In general, as the heating temperature is increased, the temperature profile becomes less uniform, although the volumetric flow rate becomes *more* uniform. Again, the point is emphasized that uniform volumetric flow rate is not required to achieve flat riser outlet temperature profiles.

Figure 5 shows the riser outlet temperature and volumetric flow rate for heating temperatures up to 3.0 with variations of $\Gamma\lambda(Re_o)$ at each temperature. The data is plotted versus the volume fraction, which is the portion of the storage volume circulated through the flow loop at any point in time, $V_f(t) = \int_0^t \dot{V}(\tau)d\tau$. It is clear that as the heating temperature is raised, the impact of the thermosyphon restriction essentially becomes a bias shift of the riser outlet temperature. The temperature profiles for high heating temperature are very similar to those for constant energy addition. Later discussion will verify that the power delivery is indeed more constant at higher heating temperature.

The effect of the flow regime also becomes more apparent at higher heating temperature. Figure 6 shows the impact of flow regime, at select values of T_h. Four distinct flow regimes are considered. At low Reynolds numbers extending up to 2300 the flow is considered laminar and the familiar Fanning friction factor result applies, $\lambda = 16/Re$. The transition regime extends from Reynolds numbers beginning at approximately 2300 and ending at approximately 4000. The loss coefficient for this type of flow is

$$\lambda = \frac{2.3 \times 10^{-8}}{Re^{-3/2}} + 0.0054, \tag{25}$$

as given by Bhatti and Shah [24]. If the flow passage is considered hydraulically smooth and the Reynolds number is greater than 4000 the flow is considered turbulent and the loss coefficient is given by the Blasius relation [25].

$$\lambda = \frac{0.0791}{Re^{1/4}}. \tag{26}$$

Finally, if the Reynolds number is greater than 4000 and the flow passage is sufficiently rough the flow is considered highly turbulent and the loss coefficient is taken to be a constant, $\lambda = c$. The impact of variable driving pressure on flow rate is reduced when the frictional losses are strongly proportional to flow rate. Based on this observation, the most favorable flow regimes are, descending in order, transitional, rough turbulent, smooth turbulent, and finally laminar flow. The results shown in Figure 6 support this conclusion, as there is a smaller decrease in volumetric flow rate for the flow regimes where frictional loss is more strongly proportional to flow rate. Particularly at high heating temperature, the more uniform flow rate results in an improved charge temperature profile.

In a manner similar to the previous two illustrations, Figure 7 displays results for the variation of the heating length at multiple high temperatures. As was the case for the flow regime and restriction geometry, the effect of the relative heating length is more apparent as the temperature of the heat source is increased. The uniformity of the riser outlet temperature

is improved for decreased heating length, although interestingly the heating length has only a very small effect on the profiles of volumetric flow rate.

The focus to this point has been on the time scale of one complete charge cycle. Emphasis on the overall charge cycle condenses the small time behavior to a small portion of the preceding illustrations. The nature of the small time scale behavior is nevertheless relevant, particularly in regards to overshoot of the setpoint and the time response of the system. The behavior of the thermosyphon system on the small time scale is dominated by inertia, quantified by the unsteady term of the momentum equation

$$\begin{matrix} R_s^2 Re \\ Gr \end{matrix} \int_0^2 \begin{pmatrix} D_r \\ D \end{pmatrix} ds. \tag{27}$$

Figure 8 shows a plot of the initial transient of the riser outlet temperature for multiple heating temperatures. The results are representative of the relevant range of parameters in the inertia term. Predictably, the overshoot is reduced for lower heating temperature.

3.3 Energy Delivery

From the preceding discussion and the results of the riser outlet temperature just presented, it appears that achieving constant volumetric flow rate is not important for low heating temperature. The riser outlet temperature profiles have shown that a uniform storage temperature can be obtained without constant flow rate. It should not come as a surprise, however, that the decay in volumetric flow rate has unfavorable consequence. This section will discuss the impact of the decaying flow rate on the rate of heat transfer to the thermosyphon fluid. The power delivery of the thermosyphon system will also be compared to the fully mixed system. In dimensionless form, the instantaneous power delivered by the thermosyphon system is computed from the expression

$$\dot{Q}(t) = \begin{matrix} \rho \hat{\dot{V}} c_p \\ \rho \hat{\dot{V}}_o c_p \Delta \hat{T}_{sp} \end{matrix} \left[\hat{T}(t, l_h) - \hat{T}(t, 0) \right] = \dot{V}(T(t, l_h) - Tt, 0). \tag{28}$$

The cumulative energy is determined by integrating the previous dimensional rate in time and scaling each of the dimensional quantities. The result is

$$Q = \frac{\int_{\hat{H}}^{2\hat{H}} \rho c_p \hat{A}_s (\hat{T}(s) - \hat{T}_o) d\hat{s}}{\rho c_p \hat{A}_s \hat{H} \Delta \hat{T}_{sp}} = \int_1^2 T(s) ds. \tag{29}$$

It was previously noted that the riser outlet temperature profiles more closely resemble constant heat addition only as the heating temperature increases. This observation is confirmed by the results shown in Figure 9 for the instantaneous heating power and cumulative energy. The power delivery is significantly more uniform at higher heating temperature and from this result it appears that higher heating temperature is unquestionably preferred. With more careful consideration, one recognizes that the higher sustained power is somewhat misleading, because much of the additional energy serves to heat the storage volume above the desired setpoint. Nevertheless, each simulation spans the time to circulate one storage volume and simulations with higher heating temperature complete this task more quickly. For comparison, the power delivery and cumulative stored energy for the fully mixed system is also shown in Figure 9. Interestingly, the power delivered by the fully mixed system and the laminar thermosyphon system at low heating temperature is nearly identical. Based on this result there is no significant benefit to the stratified thermosyphon system with laminar flow and low heating temperature, in terms of *power* delivery. Nonetheless, even though there is no advantage in terms of power delivery, the stratified storage volume of the thermosyphon system is certainly preferred over the fully mixed storage volume, since the energy is available at the desired temperature.

The similarity between the analytical result of the fully mixed system and the numerical result of the thermosyphon system suggests that the latter can be obtained analytically. In pursuit of this, the quasi-steady momentum equation is considered with the temperature

integral divided into three sections

$$\Gamma\lambda\dot{V}^2 = \int_0^1 T ds - \int_1^{1+V_f} T ds - \int_{1+V_f}^2 T ds. \tag{30}$$

For heating temperature near unity, a riser temperature equal to unity is a good approximation, therefore the first integral term evaluates to one. The second integral represents the portion of the storage volume that has been heated. Here again the temperature is assumed to be unity and as a result, the integral simplifies to the volume fraction, V_f. The remaining portion of the storage is assumed to be unheated, thereby reducing the third integral to zero. Based on these assumptions, the quasi-steady momentum equation becomes

$$\Gamma\lambda(Re)\dot{V}^2 = 1 - V_f. \tag{31}$$

Assuming the flow is laminar and the system has been designed to $\Gamma\lambda(Re_o) = 1$, the momentum equation becomes simply

$$\dot{V} = 1 - \int_0^t \dot{V} dt, \tag{32}$$

since the volume fraction is given by $V_f = \int_0^t \dot{V} dt$. Clearly, this equation admits the solution, $\dot{V} = e^{-t}$. For $T(t, l_h) \approx T_h$, the instantaneous heat transfer rate is $\dot{Q} = \dot{V} T_h$. This result is identical to the time dependent function for power delivery developed analytically for the fully mixed system. An important note however, is that this result is only applicable for T_h near unity.

The decay of power delivered to the fluid by the thermosyphon system is directly attributable to the decline in the volumetric flow rate. The mechanisms influencing the uniformity of the flow rate have already been discussed. They are the flow regime in the loss component and to lesser extent, the relative height of the heating section. The influence of these two characteristics on power is given by Figures 10 and 11. The power delivery

of the fully mixed system is again included for comparison. For low heating temperature, T_h, Figure 10 indicates that the relative height of the heating section has only a small effect on power delivery. This outcome is consistent with the conclusion that heating length has a small influence on flow rate. Notably, the heat exchanger design will be significantly less challenging without the need to limit its relative height. The results of Figure 11 show that the flow regime has a significant impact on power delivery. The thermosyphon system with flow through the restriction in the transition regime is a significant improvement compared to the fully mixed system.

To allow comparison between the fully mixed and stratified thermosyphon device, the plots of power delivery have been shown as a function of dimensionless time in Figures 10 and 11. The results are somewhat more enlightening when also plotted versus the volume fraction. For this reason the results of Figure 11 are replotted in Figure 12 as a function of volume fraction. This perspective of the data emphasizes the importance of flow regime and reinforces the observed benefit of targeting the transitional flow regime in the flow restriction element.

4. SUMMARY AND CONCLUSIONS

A unique thermosyphon storage device has been described and its performance has been simulated numerically. A thermosyphon is applied in such a way that heat is introduced into a storage system without large scale thermal mixing. The quality of energy is preserved and therefore it is more useful. Using appropriate dimensional scales the governing conservation equations have been made dimensionless and the pertinent parameter groups have been identified. The heat addition or charge process of the storage volume is the focus of this investigation. The primary challenges related to the charge process are achieving uniform storage temperature and delivering all available power for the entire charge cycle.

It was found that the relative temperature of the heat source impacts the uniformity of the charge profile as well as the steadiness of power delivery. Higher heating temperature

sustains high power delivery into the charge cycle, although at the expense of uniform charge temperature. The improved power delivery is also somewhat overstated because a portion of the energy is unnecessarily used to heat the storage volume above the setpoint. For the application of heat pump domestic hot water systems, the heating temperature is limited by the condensing temperature of the vapor compression system and this value is typically only marginally higher than the set point temperature. In such a scenario the most effective method of improving power delivery and charge profile is targeting the dominant flow behavior to the transitional regime. Although the relative height of the heating section is relevant for constant heat addition, it is not significant for constant *temperature* heat addition. Because the heating length has a small effect, the heat exchanger is free to occupy the entire system height allowing some flexibility in the practical implementation.

The dimensionless analysis that has been given is general and the conclusions are applicable to a design of any scale. Transitioning from a dimensionless design to a physical system is straightforward. One approach is to begin by selecting the desired dimensional temperature rise and available rate of heat input. The scale of the volumetric flow rate then follows. Having quantified the nominal flow rate, and with selection of a target flow regime and Reynolds number, the hydraulic diameter of the portions of the loop where frictional losses are dominant can be chosen. The steady form of the momentum equation can then be solved with a temperature distribution appropriate at the beginning of the charge cycle. Based on this approximation, the required length of the dominant loss components can be determined, thereby throttling the flow to achieve the desired setpoint. Selection of the storage volume size and aspect ratio allows the remaining dimensional quantities to be readily computed. These steps are identical to the process that would be used for constant heat addition. Constant temperature heat addition requires specification of a heat exchanger. This is done by first selecting the condensing temperature of the heat exchanger. Selection of the heating temperature can be guided by the observations made in this study. Upon

completion of this step, the required NTU can be computed. The design is completed by choosing a heat exchanger that can supply the required NTU.

Nomenclature

Dimensional quantities are denoted by a hat, *eg* $\hat{t}$.

Roman

A cross sectional area

c_p specific heat

D_h hydraulic diameter

F binary frictional loss function

G flow path orientation

g acceleration due to gravity

Gr Grashoff number, see equation (9)

H overall system height

J binary heat input function

k thermal conductivity

l length

NTU number of transfer units

Pe Peclet number , see equation (14)

Q cumulative heat addition

$\dot{Q}$ heating power

R_s aspect ratio

Re Reynolds number

s position

T temperature

t time

U overall heat transfer coefficient

V volume

v flow velocity

$\dot{V}$ volumetric flow rate

Greek

α thermal diffusivity

β coefficient of thermal expansion

ϵ heat exchanger effectiveness

Γ ratio between buoyant and frictional forces , see equation (11)

λ frictional loss coefficient

ν kinematic viscosity

ρ density

τ_w wall shear stress

Subscripts and Superscripts

h heating

m fully mixed

o design point or nominal condition

r restriction

s storage

sp set point

References

1. R. Greif, Natural circulation loops, ASME J. Heat Transfer, vol. 110, pp. 1243–1258, 1988.

2. J. W. McMenamy and K. O. Homan, Transient behavior of a free convection loop communicating with a finite reservoir, Int. J. Heat and Fluid Flow, in review.

3. K. O. Homan, Thermodynamic optimization of system configuration for electric water heating with storage: fully-mixed store, in Proceedings of the ASME Advanced Energy Systems Division, pp. 479–491, 2001.

4. B. Gebhart, Y. Jaluria, and R. L. M. B. Sammakia, Buoyancy-induced flows and transport, Hemisphere Publishing Corporation, 1988.

5. K. E. Torrance, Open-loop thermosyphons with geological applications, ASME J. Heat Transfer, vol. 101, pp. 677–683, 1979.

6. K. E. Torrance and V. W. C. Chan, Heat transfer by a free convection loop embedded in a heat-conducting solid, Int. J. Heat Mass Transfer, vol. 23, pp. 1091–1097, 1980.

7. H. H. Bau and K. E. Torrance, On the stability and flow reversal of an asymmetrically heated open convection loop, Journal of Fluid Mechanics, vol. 106, pp. 417–433, 1981.

8. H. F. Creveling, J. F. D. Paz, J. Y. Baladi, and R. J. Schoenhals, Stability characteristics of a single-phase free convection looplity characteristics of a single-phase free convection loop, Journal of Fluid Mechanics, vol. 67, pp. 65–84, 1975.

9. R. Greif, Y. Zvirin, and A. Mertol, The transient and stability behavior of a natural convection loop, ASME J. Heat Transfer, vol. 101, pp. 684–688, 1979.

10. P. S. Damerell and R. J. Schoenhals, Flow in a toroidal thermosyphon with angular displacement of heated and cooled sections, ASME J. Heat Transfer, vol. 101, pp. 672–676, 1979.

11. M. Sen, E. Ramos, and C. Trevino, The toroidal thermosyphon with known heat flux, Int. J. Heat Mass Transfer, vol. 28, pp. 219–233, 1985.

12. P. K. Yuen and H. H. Bau, Optimal and adaptive control of chaotic convection - theory and experiments, Physics of Fluids, vol. 11, pp. 1435–1448, 1999.

13. G. Muscato and M. Xibilia, Modeling and control of a natural circulation loop, Journal of Process Control, vol. 13, pp. 239–251, 2003.

14. T. N. Swift, J. A. Miller, and D. C. Hittle, A systematic approach to improving thermosyphon sdhw model performance, in Solar Engineering 1996, Proceedings of ASME Solar Energy Division Conference, pp. 165–171, 1996.

15. J. D. Burch and K. M. Gawlik, Using an ersatz thermosiphon loop to model natural convection flows inside a shallow enclosure, in Proceedings of Solar 2001, pp. 183–190, 2001.

16. A. Mertol, W. Place, T. Webster, and R. Greif, Detailed loop model analysis of liquid solar thermosyphons with heat exchangers, Solar Energy, vol. 27, pp. 367–386, 1981.

17. G. L. Morrison and J. E. Braun, System modeling and operation characteristics of thermosyphon solar water heaters, Solar Energy, vol. 34, pp. 389–405, 1985.

18. Y. Zvirin, A. Shitzer, and A. Bartal-Bornstein, On the stability of the natural circulation solar heater, in International Heat Transfer Conference, vol. 2, pp. 141–151, Hemisphere Publishing Corp., 1978.

19. P. Ranganathan, Z. Vafa, R. Schoenhals, and F. Gilleland, An experimental and analytical study of a thermosiphon-type thermal energy storage system, in Proceedings of The Seventh International Heat Transfer Conference, vol. 6, pp. 479–484, 1982.

20. S. Furbo, N. K. Vejen, and L. J. Shah, Thermal performance of a large low flow solar heating system with a highly thermally stratified tank, ASME J. Solar Energy Engineering, vol. 127, pp. 15–20, 2005.

21. A. M. Boies and K. O. Homan, Improving discharge characteristics of indirect integral collector storage systems with multi-element storage, ASME J. Solar Energy Engineering, in press.

22. K. S. Benne and K. O. Homan, Dynamics of a closed loop thermosyphon incorporating thermal storage, Numerical Heat Transfer, vol. In Review, 2007.

23. B. van Leer, Towards the ultimate conservative difference scheme. iv. a new approach to numerical convection, Journal of Computational Physics, vol. 23, pp. 276–299, 1977.

24. M. S. Bhatti and R. K. Shah, Handbok of Single-Phase Convective Heat Transfer, John Wiley & Sons, 1987.

25. H. Schlichting, Boundary Layer Theory, McGraw-Hill, 1987, seventh ed.

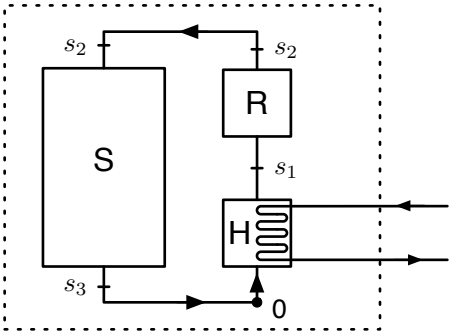

Figure 1 A conceptual schematic of the thermosyphon configuration.

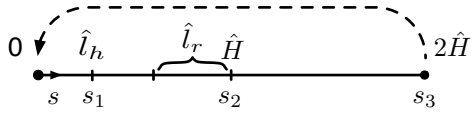

Figure 2 A linear schematic of the quasi one-dimensional thermosyphon model.

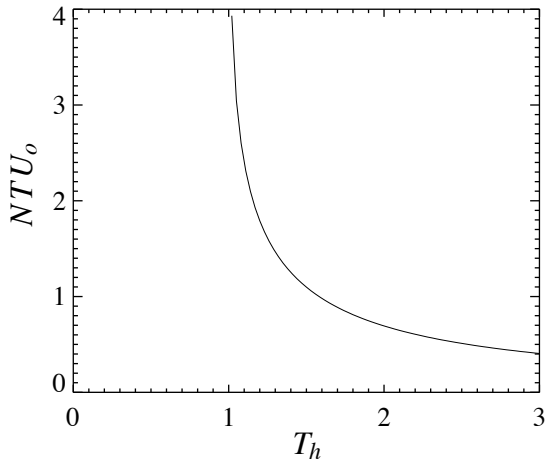

Figure 3 Required heat exchanger NTU of the thermosyphon storage system versus T_h, the dimensionless heating temperature.

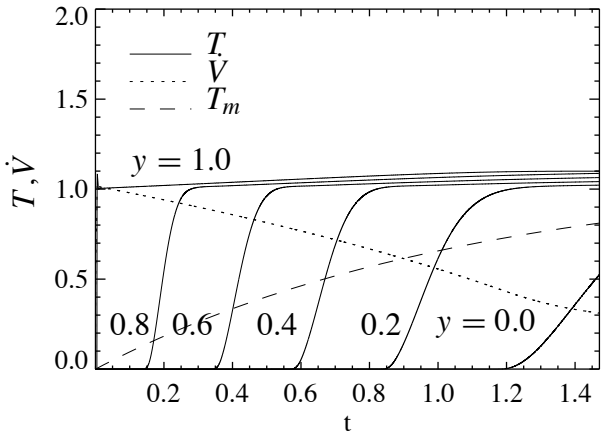

Figure 4 Traces of volumetric flowrate and temperature for the stratified thermosyphon system. Temperature is given at the riser outlet and at five evenly spaced vertical locations within the storage volume. The coordinate, $y = 0.0$, represents a location at the bottom of the storage, whereas the coordinate $y = 1.0$ represents the riser outlet temperature, and effectively the temperature in the upper most portion of the storage. The transient temperature of the fully mixed system, T_m, is included for comparison.

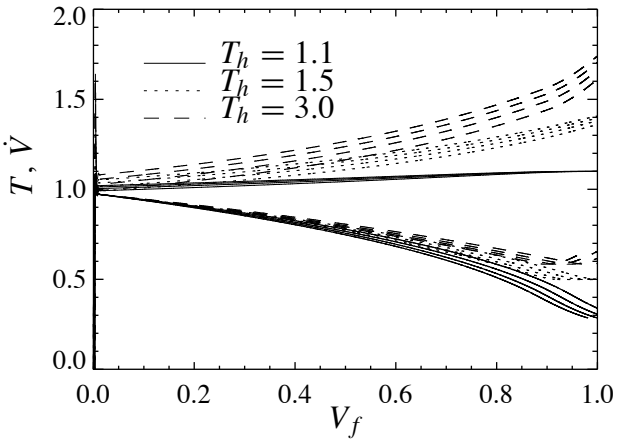

Figure 5 Thermosyphon riser outlet temperature and volumetric flow rate at multiple heating temperatures, $T_h = 1.1, 1.5, 3$. For each heating temperature, four simulations are shown with variation of the parameter group $\Gamma\lambda(Re_o)$. The values of $\Gamma\lambda(Re_o)$ are 1.11, 1.00, $1-l_h/2$, and 0.78. Larger values correspond to more restricted flow, resulting in lower volumetric flow rate and higher temperatures.

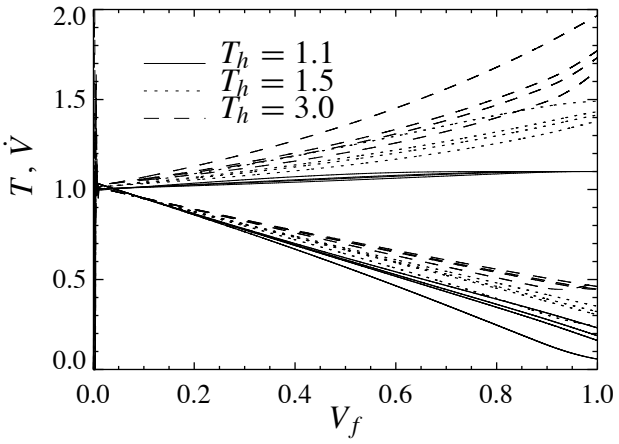

Figure 6 Thermosyphon riser outlet temperature and volumetric flow rate at multiple heating temperatures, $T_h = 1.1, 1.5, 3$. For each heating temperature, the laminar, transitional, smooth turbulent, and rough turbulent regimes are shown. The most uniform profiles are obtained by the transitional flow regime.

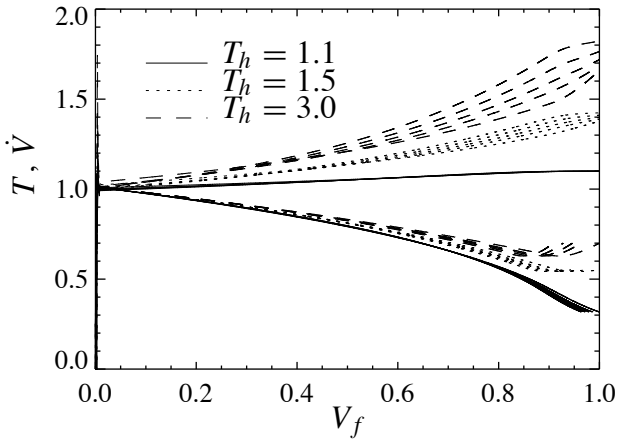

Figure 7 Thermosyphon riser outlet temperature and volumetric flow rate at multiple heating temperatures, $T_h = 1.1, 1.5, 3$. For each heating temperature, five simulations are shown with variation of the dimensionless heating length. The heating length values are 0.15, 0.35, 0.45, 0.55, and 0.65. At high heating temperature shorter length produces more uniform temperature profiles. The volumetric flow rate is affected a only small amount by heating length.

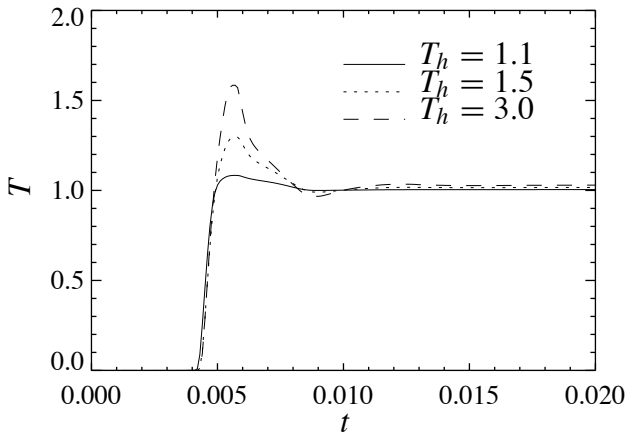

Figure 8 Riser outlet temperature at high temperatures, $T_h = 1.1, 1.5, 3$.

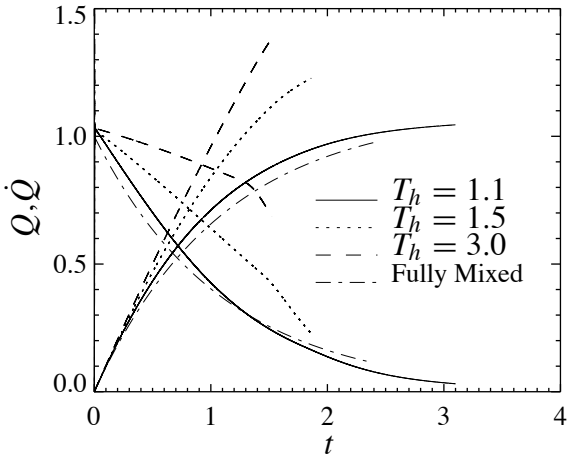

Figure 9 Heating power and cumulative energy delivered by the thermosyphon system in the laminar regime. For comparison, the power and cumulative energy is also shown for the fully mixed system with heating temperature, $T_h = 1.1$. The thermosyphon is simulated at $T_h = 1.1, 1.5, 3$. The power curves are the decreasing functions and the cumulative energy are the increasing functions. Each simulation spans one complete charge cycle.

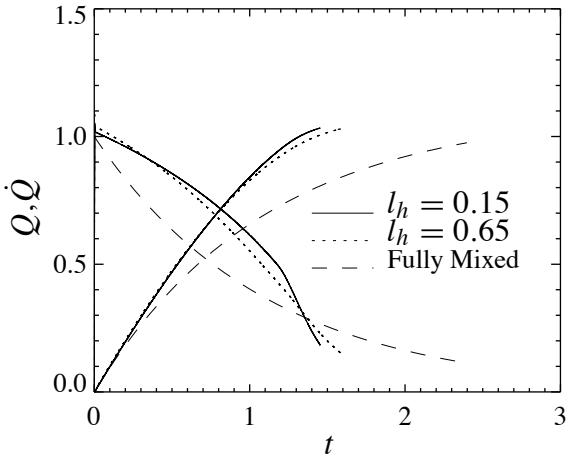

Figure 10 Heating power and cumulative energy delivered by the thermosyphon system in the transitional regime. The heating lengths are 0.15 and 0.65. For comparison, the power and cumulative energy is also shown for the fully mixed system. The heating temperature is 1.1 for all simulations. Each simulation spans one complete charge cycle.

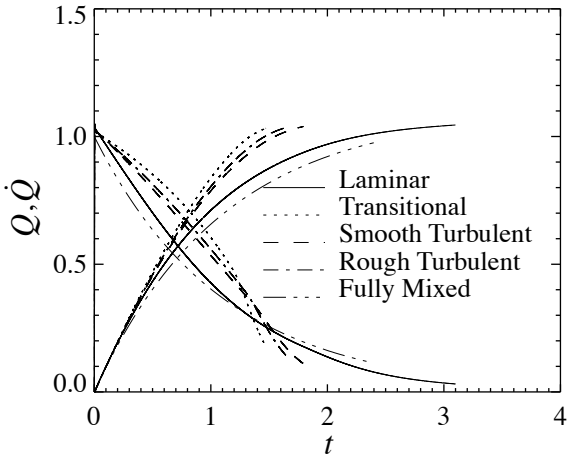

Figure 11 Heating power and cumulative energy delivered by the thermosyphon system for four distinct flow regimes. For comparison power and cumulative energy is also shown for the fully mixed system. The heating temperature is 1.1 for all simulations. Each simulation spans one complete charge cycle.

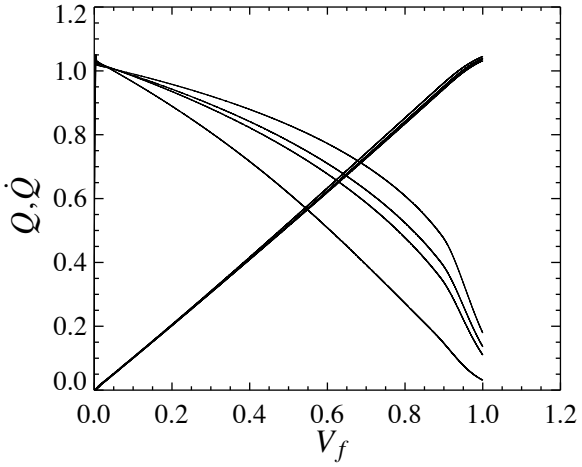

Figure 12 Heating power and cumulative energy delivered by the thermosyphon system for four distinct flow regimes. The data is identical to Figure 11 only the abscissa is volume fraction to emphasize the effect of flow regime.

APPENDIX

Page

Chapter 1

Preface

This Appendix is composed of two FORTRAN programs developed for the investigations of this thesis. The the main programs and each subprogram are contained within code "chunks" preceded by any relevant documentation. In practice a software tool, `noweb`, is used to strip the relevant code chunks out of the documentation and then assemble the necessary pieces into a completed source program. A flow diagram of the main program is illustrated by Figure 1.1.

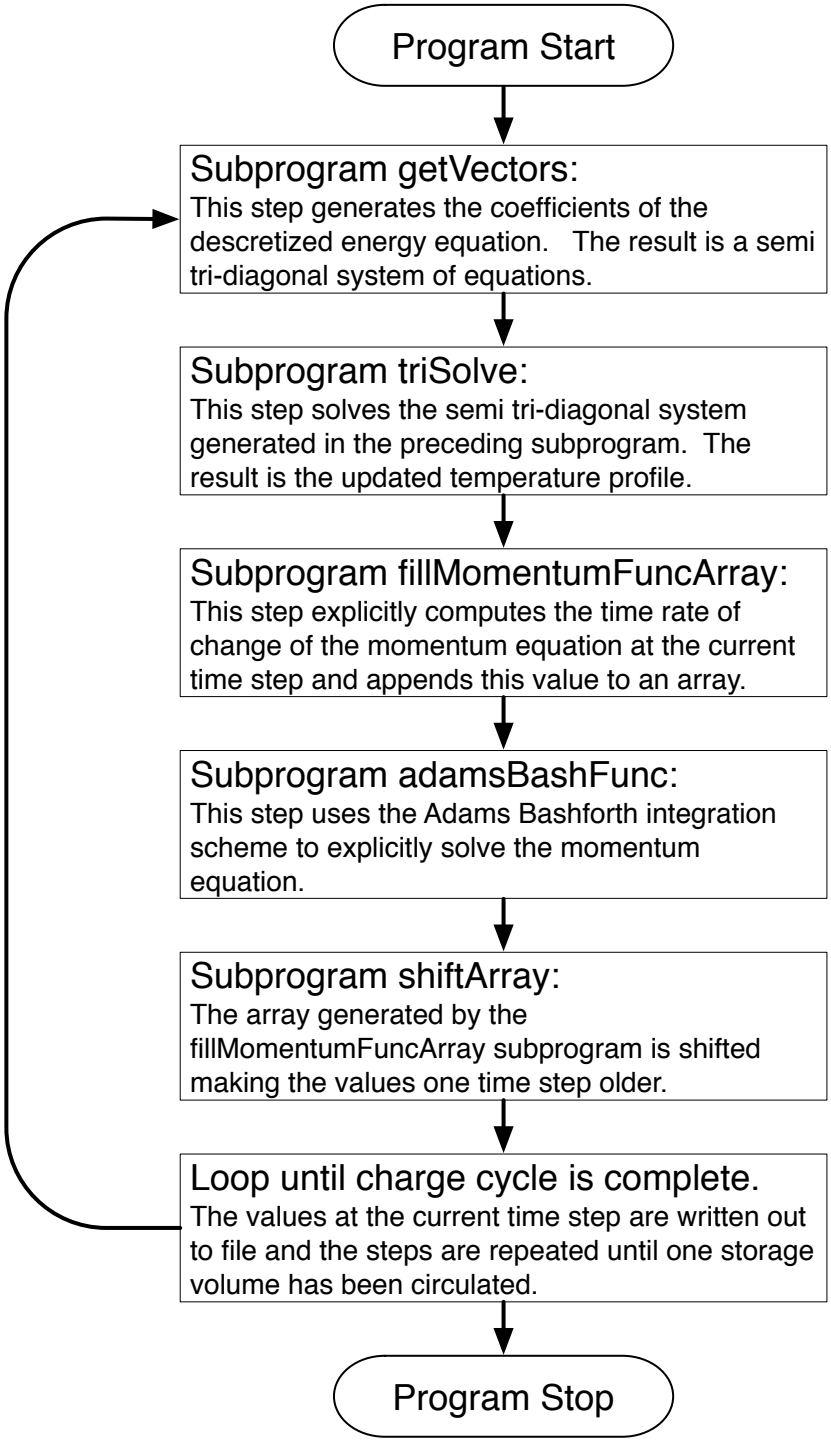

Figure 1.1: Flow diagram of the main FORTRAN program used in this study.

Chapter 2

Common Makefiles

2.1 Generic Makefile using gfortran

The compile procedure used to build the source code is scripted using GNU Make. The makefile uses the freely available gfortran compiler.

81 ⟨*makefile using gfortran* 81⟩≡

```
# ... GNU Make for the Bourne Shell ...
SHELL = /bin/sh
# ... variable declarations ...
SOURCE = prog.f90 mod.f90
EXBL   = prog.exe
F95    = gfortran
# ... compile rules ...
all : prog.exe
         -rm -f *.out
         ./$(EXBL)
         touch all

prog.exe : prog.o
        $(F95) -fdefault-real-8 -o prog.exe prog.o mod.o

prog.o : prog.f90 mod.o
        $(F95) -fdefault-real-8 -c prog.f90

mod.o : mod.f90
        $(F95) -fdefault-real-8 -c mod.f90


help :
         @echo "make     -> compile executable"
         @echo "make all -> compile and execute"
```

Chapter 3

Program `thermosyphon01`

3.1 Introduction

Program `thermosyphon01` is used in the first investigation of this thesis where constant heat addition is supplied to the thermosyphon storage device. This program numerically solves the appropriate momentum and energy equations. The energy equation is solved using a second order accurate implicit technique using the mpl method to approximate the advection term. This program time lags the momentum equation, which is solved explicitly using the Adams Bashforth method.

3.2 Program Input

Program input is provided by a chunk of FORTRAN code that declares the parameters of each numerical simulation.

3.3 Program Output

Program output is given in the form of text files that provide temperature and volumetric flow rate during the transient simulation.

3.4 Makefiles

82 ⟨*makefile to build program thermosyphon01 using gfortran* 82⟩≡
⟨*makefile using gfortran* 81⟩

3.5 Data Production Sets

Each “data production set” is composed of a chunk of input code, the program source code, a makefile, and FORTRAN module that declares a new data structure that facilitates moving the parameters throughout the program.

3.5.1 num110

Data production set `num110` serves as an example.

83a ⟨*num110params* 83a⟩≡

```
real :: Re_o=2300
real :: WHatdot_e=4500
real :: DeltaTHat_sp=42.8
real :: R_a=3.25
real :: VHat=0.1514
real :: c=0.
real :: lossFactor=1.
real, dimension(4) :: D=(/0.075,0.075,-1.,1./)
real, dimension(4) :: l=(/0.23,-1.,-2.,1./)
integer :: spec_regime=1
integer :: numI=1000
integer :: order=2
```

83b ⟨*num110prog* 83b⟩≡

⟨*program thermosyphon01* 83e⟩

83c ⟨*num110make* 83c⟩≡

⟨*makefile to build program thermosyphon01 using gfortran* 82⟩

83d ⟨*num110mod* 83d⟩≡

⟨*module for program thermosyphon01* 83f⟩

3.6 Program `thermosyphon01` Code

83e ⟨*program thermosyphon01* 83e⟩≡

⟨*program statements for program thermosyphon01* 84⟩

83f ⟨*module for program thermosyphon01* 83f⟩≡

```
module mod

type parameters !parameter types
        real :: Gr,R_a,Re_o,c,Pe,dx,dt
        real, dimension(4) :: D,l
        integer :: numI,regime,order
end type parameters

contains
```

⟨*subroutine fillMomentumFuncArray for program thermosyphon01* 86⟩

⟨*function getG for program thermosyphon01* 88b⟩

⟨*subroutine shiftArray for program thermosyphon01* 85⟩

⟨*function adamsBashFunc for program thermosyphon01* 88a⟩

⟨*subroutine triSolve for program thermosyphon01* 91⟩

⟨*subroutine getVectors for program thermosyphon01* 92⟩

⟨*function getJ for program thermosyphon01* 90⟩

⟨*subroutine mpl for program thermosyphon* 93⟩
⟨*subroutine getParams for program thermosyphon* 94⟩
⟨*function getD for program thermosyphon01* 89b⟩
⟨*function integrate for program thermosyphon01* 89a⟩
```
end module mod
```

3.6.1 Program Statements

84 ⟨*program statements for program thermosyphon01* 84⟩≡
```
program thermosyphon01

use mod

implicit none

integer :: n,i
real :: Vdot,adamsBashFunc,writeTime,V
real, dimension(:), allocatable :: T,momentumFuncArray
real, dimension(:), allocatable :: e,f,g,r
type(parameters) :: params

call getParams(params)

! allocate variables that depend on the number of nodes
! or the order of the solution method
allocate(momentumFuncArray(params%order))
allocate(T(0:params%numI+1))
allocate(e(params%numI),f(params%numI),g(params%numI),r(params%numI))

! set the initial conditions
T=0
Vdot=0
V=0
n=0

! open files for writing
writeTime=0
open(unit=11, file='regime.out', status='new')
open(unit=12, file='temps.out', status='new')
open(unit=13, file='finalTankTemp.out', status='new')

! loop through time
do
        ! count the number of iterations
        n=n+1
        ! if the volume fraction is greater than 1, stop
        if (V>1.0) exit
```

```
        ! get the e,f,g,r vectors corresponding to the energy equation
        call getVectors(e,f,g,r,T,Vdot,params)
        ! solve the energy equation implicitly to get latest T
        call triSolve(e,f,g,r,T)
        ! compute the momentum function
        call fillMomentumFuncArray(momentumFuncArray,T,Vdot,params)
        ! solve the momentum equation with the adams bashforth routine
        Vdot=adamsBashFunc(n,Vdot,momentumFuncArray,params%dt,params%order)
        ! shift the elements in the momentum function array
        call shiftArray(momentumFuncArray,params%order)
        ! record volume fraction
        V=V+Vdot*params%dt
        ! write data for current time
        ! notice writing 1000 points per 1 unit of scaled time
        if (writeTime-n*params%dt<0.1*params%dt) then
                write(11,*) n*params%dt,V,Vdot*params%Re_o,params%regime,Vdot
                write(12,*) n*params%dt,V,T(nint(params%numI*.1)),&
                        &T(nint(params%numI*.2)),&
                        &T(nint(params%numI*.3)),T(nint(params%numI*.4)),&
                        &T(nint(params%numI*.5)),T(nint(params%numI*.6)),&
                        &T(nint(params%numI*.7)),T(nint(params%numI*.8)),&
                        &T(nint(params%numI*.9)),T(params%numI)
                writeTime=writeTime+1.0/10000.
        end if
end do

! write out final tank temperatures
do i=nint(1.0/params%dx),nint(2.0/params%dx)
        write(13,*) i*params%dx,T(i)
end do

! housekeeping
deallocate(momentumFuncArray)
deallocate(T)
deallocate(e,f,g,r)

close(11)
close(12)
close(13)

end program
```

3.6.2 subroutine `shiftArray`

85 ⟨*subroutine shiftArray for program thermosyphon01* 85⟩≡

```
        subroutine shiftArray(momentumFuncArray,order)
        implicit none
```

```
        real, dimension(:) :: momentumFuncArray
        integer :: n,order

        ! shift values for momentum function
        do n=1,order-1
                momentumFuncArray(n)=momentumFuncArray(n+1)
        end do

        end subroutine
```

3.6.3 Subroutine `fillMomentumFuncArray`

86 ⟨*subroutine fillMomentumFuncArray for program thermosyphon01* 86⟩≡

```
subroutine fillMomentumFuncArray(momentumFuncArray,T,Vdot,params)

implicit none

real, dimension(:) :: momentumFuncArray
real, dimension(0 :) :: T
real, dimension(:), allocatable :: func
real :: Vdot,lambda,lGeoRatio,loss,getG,integrate,dHead
real :: iGeoRatio,inertia,Re
real, dimension(4) :: F_s,G_s
integer :: sec,i,regime
type(parameters) :: params

F_s=(/0,0,1,0/)
G_s=(/1,1,1,-1/)
allocate(func(params%numI))

Re=Vdot*params%Re_o

! if params%regime < 0, choose regime based on Re
! note that params%regime is the specified regime
if (params%regime < 0) then
        if (Re > 4000.) then
                regime=3
        else if (Re > 2300.) then
                regime=2
        else if (Re >= 0.) then
                regime=1
        end if
else
        regime=params%regime
end if
! define lambda
```

```
if (Re < 100) then
        lambda = 0.
else if (regime == 1) then
        lambda=(16./Re+params%c)
else if (regime == 2) then
        lambda=2.3E-8/Re**(-3.0/2.0)+0.0054+params%c
else if (regime == 3) then
        lambda=0.0791/Re**0.25+params%c
else if (regime == 4) then
        lambda=params%c
end if


! compute the geometry ratio in loss term
lGeoRatio=0
do sec=1,4
        lGeoRatio=lGeoRatio+params%D(3)**2.0/&
                &params%D(sec)**5.0*F_s(sec)*params%l(sec)
end do

! compute the loss term
loss=-2.0*params%R_a**3.0*params%Re_o**2.0/&
        &params%Gr*lGeoRatio*lambda*Vdot**2.0

! compute the driving head
do i=1,params%numI
        func(i)=T(i)*getG(i,G_s,params%l,params%dx)
end do
dHead=integrate(func,params%dx,params%numI)

! compute the geometry ratio of the inertia term
iGeoRatio=0
do sec=1,4
        iGeoRatio=iGeoRatio+params%D(3)**2.0/params%D(sec)**2.0*params%l(sec)
end do

! compute the inertia coefficient
inertia=params%R_a**2.0*params%Re_o**2.0/params%Gr*iGeoRatio

! output new momentum function
momentumFuncArray(params%order)=(loss+dHead)/inertia

! clean up
deallocate(func)
end subroutine
```

3.6.4 Subroutine `adamsBashFunc`

88a ⟨*function adamsBashFunc for program thermosyphon01* 88a⟩≡

```
function adamsBashFunc(n,y,yFuncArray,dt,order)
implicit none

real :: adamsBashFunc,dt
real, intent(in) :: y
integer, intent(in) :: n,order
real, intent(in), dimension(:) :: yFuncArray

integer :: m,r
real, dimension(6,0:5) :: betaArray
real :: sum


! dfine beta coefficients for Adams Bashforth method
betaArray(1,:)=(/ 1.0,0.,0.,0.,0.,0. /)
betaArray(2,:)=(/ 3./2.,-1./2.,0.,0.,0.,0. /)
betaArray(3,:)=(/ 23./12.,-16./12.,5./12.,0.,0.,0. /)
betaArray(4,:)=(/ 55./24.,-59./24.,37./24.,-9./24.,0.,0. /)
betaArray(5,:)=(/ 1901./720.,-2774./720.,2616./720.,&
                &-1274./720.,251./720.,0. /)
betaArray(6,:)=(/ 4277./1440.,-7923./1440.,9982./1440.,&
                &-7298./1440.,2877./1440.,-475./1440. /)

sum=0.
r=order
! if order requested is higher then the number of the iteration
! reduce the order
if (n-order<0) then
        r=n
end if
! compute sum in Adams Bashforth formula
do m=0,r-1
        sum=sum+betaArray(r,m)*yFuncArray(order-m)
end do

! return updated value of dependent variable
adamsBashFunc=y+dt*sum

end function
```

3.6.5 Function `getG`

88b ⟨*function getG for program thermosyphon01* 88b⟩≡

```
function getG(i,G_s,l,dx)
implicit none
```

```
real :: getG,sum,dx
real, dimension(4) :: G_s,l
integer :: i,n

sum=0
do n=1,8
        sum=sum+l(n)
        if (i*dx<sum+dx/5.) then
                getG=G_s(n)
                return
        end if
end do
end function
```

3.6.6 Function `integrate`

89a ⟨*function integrate for program thermosyphon01* 89a⟩≡

```
function integrate(f,dx,numI)
implicit none

real :: integrate,oddSum,evenSum,dx
real, dimension(:) :: f
integer :: numI,i

oddSum=0.
evenSum=0.

do i=1,numI-1,2
        oddSum=oddSum+f(i)
end do
do i=2,numI-2,2
        evenSum=evenSum+f(i)
end do
integrate=dx*(2*f(numI)+4*oddSum+2*evenSum)/3.

end function
```

3.6.7 Function `getD`

89b ⟨*function getD for program thermosyphon01* 89b⟩≡

```
function getD(i,numI,D,l,dx)
implicit none

real :: getD
real, dimension(4) :: D,l
integer, intent(in) :: i,numI
```

```
real :: sum,xSect,dx
integer :: n,section,numSec

numSec=4

! check to see if we are not looking for the ends
if (i==0) then
        getD=D(numSec)
        return
else if (i==numI+1) then
        getD=D(1)
        return
end if

! check to see what section i is in
xSect=0.
section=1
do n=1,numSec
        ! xSect holds the distance from x=0 to end of section
        xSect=xSect+l(n)
        if ((i*dx) .LE. (xSect+dx/2.)) then
                section=n
                exit
        end if
end do
! output D for that section
getD=D(section)

end function
```

3.6.8 Function `getJ`

90 ⟨*function getJ for program thermosyphon01* 90⟩≡

```
function getJ(i,J_s,l,dx)
implicit none

real :: getJ
integer, intent(in) :: i
real, dimension(4) :: l,J_s
real :: sum,xSect,dx
integer :: n,section,numSec

numSec=4

! check to see what section i is in
xSect=0.
do n=1,numSec
```

```
        ! xSect holds the distance from x=0 to end of section
        xSect=xSect+l(n)
        if ((i*dx) .LE. (xSect+dx/2.)) then
                section=n
                exit
        end if
end do
! output D for that section
getJ=J_s(section)

end function
```

3.6.9 Subroutine `triSolve`

91 ⟨*subroutine triSolve for program thermosyphon01* 91⟩≡

```
subroutine triSolve(e,f,gg,r,T)
implicit none

real, dimension(:) :: e,f,gg,r
real, dimension(0 :) :: T
real, dimension(:), allocatable :: rightVect
real :: fact,LL
integer :: i,numI

numI=size(e)

allocate(rightVect(numI))

LL=gg(numI)
rightVect=0.
rightVect(1)=e(1)
rightVect(numI-1)=gg(numI-1)
rightVect(numI)=f(numI)

! elliminate the diagonal e's
do i=2,numI-1
        fact=e(i)/f(i-1)
        f(i)=f(i)-fact*gg(i-1)
        rightVect(i)=rightVect(i)-fact*rightVect(i-1)
        r(i)=r(i)-fact*r(i-1)
end do
fact=e(numI)/f(numI-1)
rightVect(numI)=rightVect(numI)-fact*rightVect(numI-1)
r(numI)=r(numI)-fact*r(numI-1)

! elliminate the lower left term LL
do i=1,numI-2
```

```
        fact=LL/f(i)
        LL=-1*fact*gg(i)
        rightVect(numI)=rightVect(numI)-fact*rightVect(i)
        r(numI)=r(numI)-fact*r(i)
end do
fact=LL/f(numI-1)
rightVect(numI)=rightVect(numI)-fact*rightVect(numI-1)
r(numI)=r(numI)-fact*r(numI-1)

! work from bottom up to solve system
T(numI)=r(numI)/rightVect(numI)
T(numI-1)=(r(numI-1)-&
        &rightVect(numI-1)*T(numI))/f(numI-1)
do i=numI-2,1,-1
        T(i)=(r(i)-rightVect(i)*T(numI)-&
                &gg(i)*T(i+1))/f(i)
end do

deallocate(rightVect)
end subroutine
```

3.6.10 Subroutine `getVectors`

92 ⟨*subroutine getVectors for program thermosyphon01* 92⟩≡

```
subroutine getVectors(e,f,g,r,T,Vdot,params)

implicit none

real :: D_plushalf,D_minushalf,D,Dplus,Dminus
real, dimension(:) :: e,f,g,r
real, dimension(0 :) :: T
real, dimension(:), allocatable :: av,netflux
real :: Vdot,getD,gamma,getJ
real, dimension(4) :: J_s
integer :: i
type(parameters) :: params

J_s=(/1.,0.,0.,0./)

allocate(av(params%numI))
allocate(netflux(params%numI))

! we are going to define some ghost cells
T(0)=T(params%numI)
T(params%numI+1)=T(1)

! compute the net flux for each node using the mpl method
```

```
do i=1,params%numI
        av(i)=Vdot/getD(i,params%numI,params%D,params%l,params%dx)**2.0
end do
call mpl(params%dx,params%dt,T,av,netflux,params%numI,params%D,params%l)

! compute the parameters of a tri diagonal matrix
do i=1,params%numI
        ! a few lines to get the half step areas
        D=getD(i,params%numI,params%D,params%l,params%dx)
        Dplus=getD(i+1,params%numI,params%D,params%l,params%dx)
        Dminus=getD(i-1,params%numI,params%D,params%l,params%dx)
        D_plushalf=min(D,Dplus)
        D_minushalf=min(D,Dminus)
        ! gamma, a common term
        gamma=(0.5*params%dt)/(params%Pe*D**2.*params%dx**2.)
        ! the vectors
        e(i)=-gamma*D_minushalf**2.
        f(i)=1.0+gamma*(D_plushalf**2.+D_minushalf**2.)
        g(i)=-gamma*D_plushalf**2.
        r(i)=gamma*D_minushalf**2.*T(i-1)+&
                &(1.-gamma*(D_plushalf**2.+D_minushalf**2.))*T(i)+&
                &gamma*D_plushalf**2.*T(i+1)+&
                &(getJ(i,J_s,params%l,params%dx)*params%dt)/&
                &(params%l(1)*D**2.)-netflux(i)*params%dt/params%dx
end do

end subroutine
```

3.6.11 Subroutine `mpl`

93 ⟨*subroutine mpl for program thermosyphon* 93⟩≡

```
subroutine mpl(dx,kk,qq,av,netflux,numI,D,l)
implicit none

integer i,numI
real :: dx,kk,aa,getD
real, dimension(0 :) :: qq
real, dimension(:) :: av,netflux
real, dimension(:), allocatable :: gradq,flux
real, dimension(4) :: D,l


allocate(gradq(0:numI+1))
allocate(flux(0:numI))

qq(0)=qq(numI)
qq(numI+1)=qq(1)
```

```
! calculate average gradient with monotonicity constraint
do i=1,numI
        if ((qq(i)-qq(i-1))*(qq(i+1)-qq(i)) .ge. 0) then
                gradq(i)=sign(min(2.*abs(qq(i)-qq(i-1)),&
                        &2.*abs(qq(i+1)-qq(i)),&
                        &0.5*abs(qq(i+1)-qq(i-1))),&
                        &(qq(i+1)-qq(i-1)))
        else
                gradq(i)=0.
        end if
end do
gradq(0)=gradq(numI)
gradq(numI+1)=gradq(1)

! calculate fluxes at cell faces
do i=1,numI
        aa=abs(av(i))
        if (av(i) .ge. 0.) then
                flux(i)=aa*getD(i,numI,D,l,dx)**2*(qq(i)+0.5*(1.-aa*kk/dx)*gradq(i))
        else
                flux(i)=aa*getD(i+1,numI,D,l,dx)**2*&
                        &(-qq(i+1)+0.5*(1.-aa*kk/dx)*gradq(i+1))
        end if
end do
flux(0)=flux(numI)

! calculate net convective flux
do i=1,numI
        netflux(i)=1./getD(i,numI,D,l,dx)**2*(flux(i)-flux(i-1))
end do

! housekeeping
deallocate(flux)
deallocate(gradq)

end subroutine
```

3.6.12 Subroutine `getParams`

94 ⟨*subroutine getParams for program thermosyphon* 94⟩≡

```
subroutine getParams(params)
implicit none

real :: VHatDot_o,DHat_r,DHat_t,HHat,D_r,c_p,lambda,gamma
real :: g,rho,pi,beta,nu,alpha,Gr,Pe
real :: dx,dt
```

```
integer :: regime

type(parameters) :: params

include 'params.inc'

! constants
g=9.81
rho=997.
pi=2.*asin(1.)
beta=2.6E-4
nu=0.87E-6
alpha=0.147E-6
c_p=4180.

! dx determined by the number of nodes specified
dx=2.0/numI

! the characteristic volumetric flowrate
VHatDot_o = WHatdot_e/(rho*c_p*DeltaTHat_sp)
! the diameter of the restriction
DHat_r=(4.0*VHatDot_o)/(pi*nu*Re_o)
! the diameter of the tank
DHat_t=((VHat*4.0)/(pi*R_a))**(1./3.)
! the height of the system
HHat=R_a*DHat_t

! the dimensionless diameter of the restriction
D_r=DHat_r/DHat_t

! the grashoff number
Gr=(g*beta*DeltaTHat_sp*HHat**3.)/nu**2.0

! the peclet number
Pe=(4.0*VHatDot_o*HHat)/(pi*DHat_t**2.0*alpha)

! if D(3) < 0
! set to computed value of D_r
if (D(3) < 0.) then
        D(3)=D_r
end if

! choose dt based on CFL of 0.8
dt=(0.8*dx*pi*D(3)**2)/4.

!! if regime < 0 choose regime based on Re_o
if (spec_regime < 0) then
```

```
        ! flow is turbulent
        if (Re_o > 4000. ) then
                regime=3
        ! flow is transitioning
        else if (Re_o > 2300.) then
                regime=2
        ! flow is laminar
        else if (Re_o > 0.) then
                regime=1
        end if
else
        regime=spec_regime
end if

! compute lambda at the target reynolds number
if (regime == 1) then
        lambda=(16./Re_o+c)
else if (regime == 2) then
        lambda=(2.3E-8/Re_o**(-3.0/2.0)+0.0054+c)
else if (regime == 3) then
        lambda=(0.0791/Re_o**0.25+c)
else if (regime == 4) then
        lambda=c
end if

! the length of the restriction is programmatically
! chosen to satisfy the setpoint at startup

! if set to -1 the riser is assumed to be
! at the set point temperature
if (l(3) < -0.9 .and. l(3) > -1.1) then
        l(3)=1./(2.*R_a**3.*Re_o**2./(Gr*D(3)**3.)*lambda)
! if set to -2 the riser temperature is assumed to be
! linearly increasing within the heating section
! and at the setpoint for the rest of the riser section
else if (l(3) < -1.9 .and. l(3) > -2.1) then
        l(3)=(1.-0.5*l(1))/(2.*R_a**3.*Re_o**2./(Gr*D(3)**3.)*lambda)
end if
! the length of the unheated riser section "floats"
l(2)=1.-l(1)-l(3)

! output the computed values from this subroutine in the form of a structure
params%Gr=Gr
params%Pe=Pe
params%R_a=R_a
params%Re_o=Re_o
params%l=l
```

```
params%D=D
params%c=c
params%regime=spec_regime
params%dx=dx
params%dt=dt
params%numI=numI
params%order=order

end subroutine
```

Chapter 4

Program `thermosyphon02`

4.1 Introduction

Program `thermosyphon02` is used in the second investigation of this thesis where constant temperature heat addition is supplied to the thermosyphon storage device. The program follows the same methodology as `thermosyphon01` except inputs are given that are appropriate for a constant temperature heat source and a modified energy equation is solved. Many of the subprograms are shared with `thermosyphon01`.

4.2 Program Input

Program input is provided by a chunk of FORTRAN code that declares the parameters of each numerical simulation.

4.3 Program Output

Program output is given in the form of text files that provide temperature and volumetric flow rate during the transient simulation.

4.4 Makefiles

98a ⟨*makefile to build program thermosyphon02 using gfortran* 98a⟩≡
⟨*makefile using gfortran* 81⟩

4.5 Data Production Sets

An example data production set is given for program `thermosyphon02`.

4.5.1 num210

98b ⟨*num210params* 98b⟩≡
```
real :: Re_o=2300
```

```
real :: QHatDot_o=4500
real :: DeltaTHat_sp=42.8
real :: R_a=3.25
real :: VHat=0.1514
real :: c=0.
real, dimension(4) :: D=(/0.075,0.075,-1.,1./)
real, dimension(4) :: l=(/0.25,-1.,-2.,1./)
integer :: spec_regime=1
integer :: numI=100
integer :: order=2
real :: U_o=75.
real :: T_h=1.1
```

99a ⟨*num210prog* 99a⟩≡
⟨*program thermosyphon02* 99d⟩

99b ⟨*num210make* 99b⟩≡
⟨*makefile to build program thermosyphon02 using gfortran* 98a⟩

99c ⟨*num210mod* 99c⟩≡
⟨*module for program thermosyphon02* 99e⟩

4.6 Program `thermosyphon02` Code

99d ⟨*program thermosyphon02* 99d⟩≡
⟨*program statements for program thermosyphon02* 100⟩

99e ⟨*module for program thermosyphon02* 99e⟩≡

```
module mod

type parameters !parameter types
        real :: Gr,R_a,Re_o,c,Pe,dx,dt,T_h
        real :: U_o,NTU_o
        real, dimension(4) :: D,l
        integer :: numI,regime,order
end type parameters

contains
```

⟨*subroutine fillMomentumFuncArray for program thermosyphon02* 102b⟩
⟨*function getG for program thermosyphon02* 102d⟩
⟨*subroutine shiftArray for program thermosyphon02* 102a⟩
⟨*function adamsBashFunc for program thermosyphon02* 102c⟩
⟨*subroutine triSolve for program thermosyphon02* 102h⟩
⟨*subroutine getVectors for program thermosyphon02* 103⟩
⟨*function getJ for program thermosyphon02* 102g⟩
⟨*subroutine mpl for program thermosyphon* 93⟩
⟨*subroutine getParams for program thermosyphon* 94⟩
⟨*function getD for program thermosyphon02* 102f⟩

⟨*function integrate for program thermosyphon02* 102e⟩
⟨*function U for program thermosyphon* 104b⟩
```
end module mod
```

4.6.1 Program Statements

100 ⟨*program statements for program thermosyphon02* 100⟩≡
```
program thermosyphon02

use mod

implicit none

integer :: n,i,Iriser
real :: tank_int,riser_int
real :: Vdot,adamsBashFunc,writeTime,V,inst_power,tot_E
real, dimension(:), allocatable :: T,momentumFuncArray
real, dimension(:), allocatable :: e,f,g,r
type(parameters) :: params

call getParams(params)

! allocate variables that depend on the number of nodes
! or the order of the solution method
allocate(momentumFuncArray(params%order))
allocate(T(0:params%numI+1))
allocate(e(params%numI),f(params%numI),g(params%numI),r(params%numI))

! set the initial conditions
T=0
Vdot=0
V=0
n=0

! open files for writing
writeTime=0
open(unit=11, file='regime.out', status='new')
open(unit=12, file='temps.out', status='new')
open(unit=13, file='finalTankTemp.out', status='new')
open(unit=14, file='integral.out', status='new')

! loop through time
do
        ! count the number of iterations
        n=n+1
        ! if the volume fraction is greater than 1, stop
        if (V>1.0) exit
```

```
        ! get the e,f,g,r vectors corresponding to the energy equation
        call getVectors(e,f,g,r,T,Vdot,params)
        ! solve the energy equation implicitly to get latest T
        call triSolve(e,f,g,r,T)
        ! compute the momentum function
        call fillMomentumFuncArray(momentumFuncArray,T,Vdot,params)
        ! solve the momentum equation with the adams bashforth routine
        Vdot=adamsBashFunc(n,Vdot,momentumFuncArray,params%dt,params%order)
        ! shift the elements in the momentum function array
        call shiftArray(momentumFuncArray,params%order)
        ! record volume fraction
        V=V+Vdot*params%dt
        ! write data for current time
        ! notice writing 1000 points per 1 unit of scaled time
        if (writeTime-n*params%dt<0.1*params%dt) then
                write(11,*) n*params%dt,V,Vdot*params%Re_o,params%regime,Vdot
                write(12,*) n*params%dt,V,T(nint(params%numI*.1)),&
                        &T(nint(params%numI*.2)),&
                        &T(nint(params%numI*.3)),T(nint(params%numI*.4)),&
                        &T(nint(params%numI*.5)),T(nint(params%numI*.6)),&
                        &T(nint(params%numI*.7)),T(nint(params%numI*.8)),&
                        &T(nint(params%numI*.9)),T(params%numI)
                writeTime=writeTime+1.0/10000.
                inst_power=Vdot*(T(nint(params%numI/2*params%l(1)))-&
                        &T(0))
                Iriser=nint(1.0/params%dx)
                tank_int=integrate(T(Iriser+1:params%numI),&
                        &params%dx,params%numI-Iriser)
                riser_int=integrate(T(1:Iriser),params%dx,Iriser)
                write(14,*) n*params%dt,inst_power,tank_int,riser_int
        end if
end do

! write out final tank temperatures
do i=nint(1.0/params%dx),nint(2.0/params%dx)
        write(13,*) i*params%dx,T(i)
end do

! housekeeping
deallocate(momentumFuncArray)
deallocate(T)
deallocate(e,f,g,r)

close(11)
close(12)
close(13)
```

```
end program
```

4.6.2 subroutine `shiftArray`

102a ⟨*subroutine shiftArray for program thermosyphon02* 102a⟩≡
⟨*subroutine shiftArray for program thermosyphon01* 85⟩

4.6.3 Subroutine `fillMomentumFuncArray`

102b ⟨*subroutine fillMomentumFuncArray for program thermosyphon02* 102b⟩≡
⟨*subroutine fillMomentumFuncArray for program thermosyphon01* 86⟩

4.6.4 Subroutine `adamsBashFunc`

102c ⟨*function adamsBashFunc for program thermosyphon02* 102c⟩≡
⟨*function adamsBashFunc for program thermosyphon01* 88a⟩

4.6.5 Function `getG`

102d ⟨*function getG for program thermosyphon02* 102d⟩≡
⟨*function getG for program thermosyphon01* 88b⟩

4.6.6 Function `integrate`

102e ⟨*function integrate for program thermosyphon02* 102e⟩≡
⟨*function integrate for program thermosyphon01* 89a⟩

4.6.7 Function `getD`

102f ⟨*function getD for program thermosyphon02* 102f⟩≡
⟨*function getD for program thermosyphon01* 89b⟩

4.6.8 Function `getJ`

102g ⟨*function getJ for program thermosyphon02* 102g⟩≡
⟨*function getJ for program thermosyphon01* 90⟩

4.6.9 Subroutine `triSolve`

102h ⟨*subroutine triSolve for program thermosyphon02* 102h⟩≡
⟨*subroutine triSolve for program thermosyphon01* 91⟩

4.6.10 Subroutine `getVectors`

103 ⟨*subroutine getVectors for program thermosyphon02* 103⟩≡

```
subroutine getVectors(e,f,g,r,T,Vdot,params)

implicit none

real :: D_plushalf,D_minushalf,D,Dplus,Dminus
real, dimension(:) :: e,f,g,r
real :: Re,U
real, dimension(0 :) :: T
real, dimension(:), allocatable :: av,netflux
real :: Vdot,getD,gamma,eta,getJ
real, dimension(4) :: J_s
integer :: i
type(parameters) :: params

J_s=(/1.,0.,0.,0./)

allocate(av(params%numI))
allocate(netflux(params%numI))

! we are going to define some ghost cells
T(0)=T(params%numI)
T(params%numI+1)=T(1)

! the true Reynolds number
Re=Vdot*params%Re_o

! compute the net flux for each node using the mpl method
do i=1,params%numI
        av(i)=Vdot/getD(i,params%numI,params%D,params%l,params%dx)**2.0
end do
call mpl(params%dx,params%dt,T,av,netflux,params%numI,params%D,params%l)

! compute the parameters of a tri diagonal matrix
do i=1,params%numI
        ! a few lines to get the half step areas
        D=getD(i,params%numI,params%D,params%l,params%dx)
        Dplus=getD(i+1,params%numI,params%D,params%l,params%dx)
        Dminus=getD(i-1,params%numI,params%D,params%l,params%dx)
        D_plushalf=min(D,Dplus)
        D_minushalf=min(D,Dminus)
        ! gamma and eta, common terms
        gamma=(0.5*params%dt)/(D**2*params%Pe*params%dx**2.)
        eta=(params%dt*params%NTU_o*U(Re)*getJ(i,J_s,params%l,params%dx))/&
                &(params%l(1)*D**2.*params%U_o)
```

```
        ! the vectors
        e(i)=-gamma*D_minushalf**2.
        f(i)=1.0+0.5*eta+gamma*(D_plushalf**2.+D_minushalf**2.)
        g(i)=-gamma*D_plushalf**2.
        r(i)=T(i)-netflux(i)*params%dt/params%dx+&
                &eta*params%T_h-0.5*eta*T(i)+&
                &gamma*(D_plushalf**2.*T(i+1)-&
                &(D_plushalf**2.+D_minushalf**2.)*T(i)+&
                &D_minushalf**2.*T(i-1))
    end do

    end subroutine
```

4.6.11 Subroutine `mpl`

104a ⟨*subroutine mpl for program thermosyphon* 93⟩+≡
⟨*subroutine mpl for program thermosyphon* 93⟩

4.6.12 Subroutine `U`

104b ⟨*function U for program thermosyphon* 104b⟩≡

```
    function U(Re)
    implicit none

    real :: U
    real , intent(in) :: Re
    real :: a,b,c

    a=75.
    b=0.
    c=0.

    U=a/Re**b+c

    end function U
```

4.6.13 Subroutine `getParams`

104c ⟨*subroutine getParams for program thermosyphon* 94⟩+≡

```
    subroutine getParams(params)
    implicit none

    real :: VHatDot_o,DHat_r,DHat_t,HHat,D_r,c_p,lambda,gamma
    real :: g,rho,pi,beta,nu,alpha,Gr,Pe,NTU_o,AHat_h
    real :: dx,dt
    integer :: regime
```

```
type(parameters) :: params

include 'params.inc'

! constants
g=9.81
rho=997.
pi=2.*asin(1.)
beta=2.6E-4
nu=0.87E-6
alpha=0.147E-6
c_p=4180.

! dx determined by the number of nodes specified
dx=2.0/numI

! the characteristic volumetric flowrate
VHatDot_o = QHatDot_o/(rho*c_p*DeltaTHat_sp)
! the diameter of the restriction
DHat_r=(4.0*VHatDot_o)/(pi*nu*Re_o)
! the diameter of the tank
DHat_t=((VHat*4.0)/(pi*R_a))**(1./3.)
! the height of the system
HHat=R_a*DHat_t

! the dimensionless diameter of the restriction
D_r=DHat_r/DHat_t

! the grashoff number
Gr=(g*beta*DeltaTHat_sp*HHat**3.)/nu**2.0

! the peclet number
Pe=(4.0*VHatDot_o*HHat)/(pi*DHat_t**2.0*alpha)

! if D(3) < 0
! set to computed value of D_r
if (D(3) < 0.) then
        D(3)=D_r
end if

! choose dt based on CFL of 0.8
dt=(0.8*dx*pi*D(3)**2)/4.

!! if spec_regime < 0 choose regime based on Re_o
if (spec_regime < 0) then
        ! flow is turbulent
        if (Re_o > 4000. ) then
```

```
                regime=3
        ! flow is transitioning
        else if (Re_o > 2300.) then
                regime=2
        ! flow is laminar
        else if (Re_o > 0.) then
                regime=1
        end if
else
        regime=spec_regime
end if

! compute lambda at the target reynolds number
if (regime == 1) then
        lambda=(16./Re_o+c)
else if (regime == 2) then
        lambda=(2.3E-8/Re_o**(-3.0/2.0)+0.0054+c)
else if (regime == 3) then
        lambda=(0.0791/Re_o**0.25+c)
else if (regime == 4) then
        lambda=c
end if

! the length of the restriction is programmatically
! chosen to satisfy the setpoint at startup

! if set to -1 the riser is assumed to be
! at the set point temperature
if (l(3) < -0.9 .and. l(3) > -1.1) then
        l(3)=1./(2.*R_a**3.*Re_o**2./(Gr*D(3)**3.)*lambda)
! if set to -2 the riser temperature is assumed to be
! linearly increasing within the heating section
! and at the setpoint for the rest of the riser section
else if (l(3) < -1.9 .and. l(3) > -2.1) then
        l(3)=(1.-0.5*l(1))/(2.*R_a**3.*Re_o**2./(Gr*D(3)**3.)*lambda)
end if
! the length of the unheated riser section "floats"
l(2)=1.-l(1)-l(3)

! compute the rquired NTU_o
NTU_o=Log(T_h/(T_h-1.))

! output the computed values from this subroutine in the form of a structure
params%Gr=Gr
params%Pe=Pe
params%R_a=R_a
params%Re_o=Re_o
```

```
params%l=l
params%D=D
params%c=c
params%regime=regime
params%dx=dx
params%dt=dt
params%numI=numI
params%order=order
params%T_h=T_h
params%U_o=U_o
params%NTU_o=NTU_o

end subroutine
```

VITA

Kyle Stephen Benne was born on January 22, 1983 in St. Louis, Missouri. In May 2001, he graduated from Francis Howell High School in St. Charles, Missouri. During the fall of 2001, he enrolled at Central Missouri State University. The following year he transferred to the University of Missouri-Rolla (UMR) to study Mechanical Engineering. He graduated with his B.S. degree in Mechanical Engineering from UMR in May 2005. In the fall, he began his graduate work under Dr. Kelly Homan in the Mechanical Engineering department at UMR. In December of 2007, he graduated from UMR with his M.S. degree in Mechanical Engineering.